Joint Centre for Mesoscale Meteorology, Reading, UK

Use of satellite imagery to diagnose events leading to frontal thunderstorms:Parts I and II of a case study

K. A. Browning
N. M. Roberts

Internal Report No. 37

November 1994

Met Office Joint Centre for Mesoscale Meteorology Department of Meteorology
University of Reading PO Box 243 Reading RG6 6BB United Kingdom
Tel: +44 (0)118 931 8425 Fax: +44 (0)118 931 8791
www.metoffice.com

Version dated 20 October 1994

Use of satellite imagery to diagnose events leading to frontal thunderstorms: a case study

K A Browning and N M Roberts
Joint Centre for Mesoscale Meteorology, University of Reading, PO Box 240, Reading RG6 2FN, UK

Abstract

This paper presents a case study to illustrate the value of water vapour and other satellite imagery, when used in conjunction with a conceptual model, to help the forecaster identify deficiencies in numerical model forecast guidance and to diagnose what is happening on the mesoscale. The specific application discussed is the triggering of frontal thunderstorms by the pattern of overrunning and ascent associated with an upper-level vortex in the vicinity of a trailing cold front.

1. Introduction

An important process leading to frontal thunderstorms is the overrunning of dry potentially cold air over warm moist air. In terms of wet-bulb potential temperature, this corresponds to low-θ_w air overrunning high-θ_w air. The resulting potential instability is realised as deep convection if there is sufficient large-scale ascent or surface heating. A combination of this kind of overrunning and large-scale ascent occurs along parts of a front in association with cyclogenesis. Often this is well represented by numerical model guidance; occasionally it is not, and it is in these circumstances that satellite imagery can be particularly valuable in identifying what is happening.

The present paper gives an example of the use of imagery on an occasion when runs of the Meteorological Offices' operational model failed to predict the circumstances leading to an outbreak of thunderstorms over the Bay of Biscay, later spreading to the English Channel. We make use of geostationary (Meteosat) imagery because it reveals the evolution

of the situation with the necessary resolution in time. We utilize visible (VIS), infra-red (IR) and water vapour (WV) imagery but the use of the WV imagery (6.7 μm) is particularly crucial because it identifies key regions of dry upper-tropospheric air: so-called "dark" zones (Weldon & Holmes, 1991). These dark zones, in a region of cyclogenesis, correspond to low-θ_w air (the so-called dry intrusion of Young et al., 1987). After descending from near tropopause level, air in the dry intrusion overruns and ascends above a region of high-θ_w air. This is what leads, sometimes, to the outbreak of convective showers or thunderstorms.

This overrunning process is represented in the split-front model of Browning & Monk (1982) where the leading edge of the dry intrusion, referred to as an upper cold front (UCF) (strictly an upper cold θ_w-front), runs ahead of the surface boundary of the high-θ_w air, corresponding to the surface cold front (SCF). In some circumstances, notably in the region of overrunning dry air before the outbreak of deep convection, the position of the UCF can be diagnosed from the WV imagery and the position of the SCF can be diagnosed from the VIS imagery.

In Section 2 we present the broad synoptic-scale context of our case study and show how the satellite imagery reveals the UCF advancing ahead of the SCF over the Bay of Biscay. We demonstrate that the outbreak of thunderstorms occurred between the UCF and SCF. In Section 3 we show how a sequence of images viewed in a Lagrangian (i.e. system-relative) frame are able to reveal the effects of the upper-tropospheric vortex that leads to the overrunning process. In Section 4 we show a comparison between the WV imagery and the equivalent model-derived pseudo-WV imagery to demonstrate the failure of the model to represent this vortex.

There is evidence in this case of the model going wrong many hours before the thunderstorms broke out. Although it would have been difficult to have anticipated on the grounds of the imagery alone when the thunderstorms would develop, the satellite imagery nevertheless provided a useful indication of the increased likelihood of thunderstorms and of the area at risk.

2. Large-scale context of the thunderstorms and the overrunning dry intrusion

Thunderstorms first broke out in the northeast of sea-area Finisterre, in the west of the Bay of Biscay, at 1430 UTC on 27 July. They occurred in a region of high pressure (1020 mb) along a trailing cold front (Figure 1(a)). Ahead of the cold front at 900 mb (Figure 1(b)) the model shows there was a band with θ_w about 15°C associated with a warm conveyor belt and, ahead of that, there was a larger region of even higher θ_w associated with the heated land. Behind the cold front at 500 mb (Figure 1(b)), the θ_w decreased below 15°C: satellite imagery will show that it was air from this region which overran the warm boundary-layer air and led to the thunderstorms, although this overrunning was not properly represented by the model.

Satellite imagery at 1300 UTC (Figure 2) shows a well-defined cloud band along the cold front. The VIS imagery (Figure 2(a)) shows a 200 km-wide band of bright cloud (i.e. convective tops) from just off Corunna (north-west corner of Spain) to south-west England. Experience with interpreting imagery from split fronts (kata-cold fronts) suggests that, in the region of overrunning dry air, the western boundary of the bright cloud corresponds to the SCF (Browning & Monk, 1982; Browning et al., 1987). The IR image (Figure 2(b)) shows

that, over half this width, the cloud tops were moderately high (T <-30°C) to the north of latitude 45 deg. Farther south the tops were mainly warmer than O°C. The WV image (Figure 2(c)) shows a slightly waved moist band along the cold front, with very dry upper-level air (coloured dark blue) already beginning to advance over the western edge of the visible cloud band south of 45 deg. The mid-point of the main moisture gradient inferred from Figure 2(c) is taken to represent the UCF.

Figure 2(c) also shows a tell-tale hook of slightly moister air (light blue and green) to the west of the Bay of Biscay at 10°W. This is an indicator of an upper-level vorticity maximum (Browning, 1993): similar features sometimes produce a 'cloud head' (e.g. Browning & Roberts, 1994) but, as in the early stages of the case studied by Browning (1993), this one was cloud-free and we shall refer to it as a 'moist head'.

A sequence of images similar to those in Figure 2 has been analysed to reveal the advance of the UCF ahead of the SCF - see Figure 3. Figure 3(a) shows that the SCF and UCF were essentially coincident at 0630 UTC. Figure 3(b), corresponding approximately to the time of Figure 2, shows the UCF beginning to advance ahead of the SCF in the south. By 1830 UTC (Figure 3(c)), the UCF had progressed 200 km ahead of the SCF. Meanwhile, Figure 3 shows that the feature referred to as a moist head was advancing north-eastwards at about 16 m s^{-1}: we shall discuss this further in Section 3.

The region of overrunning between the UCF and SCF in the split-front model (Browning & Monk, 1982) is a potentially unstable region where deep convection may be triggered if there is sufficient large-scale ascent. Successive hourly position of this region are

plotted in Figure 4, together with locations of sferics recorded by the Met Office ATD system (Lee, 1989). It is evident that there is a close association, over the sea, between the sferics and this region, (the 60-min window for the sferics observations accounts for the sferics situated just outside of it).

One of the reasons why we chose this case to illustrate the use of imagery is because of the relative simplicity of the event, at least in its early stages. This was partly due to the lack of topographical effects at the onset of the storms. As the frontal system moved towards the continent, however, it began to draw upon low-level air with a high θ_w due to surface heating. This led to complications which we shall remark upon briefly.

The first thunderstorms, labelled A in Figure 5 broke out at 1430 and were dying out by 1800. These storms were indeed unaffected by topography. Further storms developed after 1800; these broke out farther to the south and east. This second outbreak of thunderstorms is labelled B in Figure 5. Storm Area B, unlike the earlier Storm Area A, was affected by the land mass. It developed at the UCF as soon as the leading edge of the dry intrusion began to overrun boundary-layer air with higher θ_w coming from northern Spain. Recall that the numerical model (Figure 1(b)) showed air with high θ_w at 900 mb streaming downwind from Spain. For several hours prior to the outbreak of Storm Area B this plume of warm air showed up in the imagery as an area of generally rather shallow convective cloud. The western boundary of this area can be seen in both Figure 2 and Figure 5 as a line of lower cloud tops extending from NW Spain to Brittany. This boundary remained almost stationary for several hours and its position is denoted by the dashed line in Figure 5. It was

when the UCF crossed this line that the convection was invigorated and Storm Area B began to develop.

3. An upper-level vortex and its effects

We have shown in the previous section that the thunderstorms were associated with upper-level air in the dry intrusion overrunning low-level air of high θ_w. As can be seen in Figure 3, this was associated with the UCF deforming at a faster rate than the underlying SCF, which itself remained nearly straight during much of the analysed period. Evidence from the satellite imagery suggests that the distortion of the UCF is consistent with simple rotation of the upper-level flow. The relative lack of distortion of the SCF indicates that such an effect was very much less at low levels, and only the weakest possible surface low was discernable as the system subsequently cross the English Channel. The evidence for upper-level rotation is given in Figure 6.

Figure 6(a) depicts three consecutive positions of the moist head: the arrows in Figures 6(b&c) show the velocity of the moist head, about 16 m s^{-1} from 230 deg. Figure 6(b) shows successive 6-hourly positions of the satellite-derived UCF drawn in a frame of reference moving with the moist head. The rotation of the UCF is clearly revealed.

Figure 6(c) shows successive 90-min positions of the satellite-derived anvil plume from Thunderstorm Area B, again drawn in a frame of reference moving with the moist head. The main updraughts and highest tops were at the southern end of the plume and the plume itself drifted from right to left, consistent with it being embedded within the leading portion

of a cyclonically rotating upper-level flow. As noted earlier in Section 2, the mere detection of a moist head is itself evidence of an upper-level vortex. However, it is not known how often moist heads are detectable and, in any case, the identification of a moist head is subjective and may be unreliable unless, as in this case, it is supported by other evidence in the imagery.

The above satellite evidence suggests that we should also expect evidence of an upper tropospheric maximum in vorticity (and potential vorticity, PV) in the numerical model output. Unfortunately there was no sign of such a closed maximum in the model forecasts examined for this occasion. There was a long upper-level PV-strip along the trailing cold front, extending from a major PV maximum near the cyclone centre but there was no evidence in the model of this becoming cut off to produce a local maximum. This indicates a significant deficiency in model performance on this occasion as a result of which the model runs failed to predict the outbreak of these thunderstorms over the Bay of Biscay and north-west France.

4. Use of satellite imagery to identify deficiencies in numerical model guidance

We have described a case in which the numerical model failed to produce a cut-off upper-level vortex (PV maximum) that was responsible for an outbreak of thunderstorms. We have shown how the evidence for such a vortex can be inferred from the satellite imagery. When using imagery operationally for the purpose of evaluating model performance, it is probably better to make comparisons on the basis not of highly differentiated quantities such as vorticity but rather in terms of the integrated effects of the vorticity, such as the distortion

of relative humidity gradients. Indeed the most straightforward procedure is to compare the WV imagery with the corresponding model-derived relative humidity patterns in the region of dry intrusions. The simplicity of this comparison arises because the model-derived patterns corresponding to cloud-free parts of the WV images do not depend on parameterized processes such as cloud production. Sometimes this simple comparison between imagery and model is confused by the dry intrusion going beneath high-level cirrus. This did not happen in the present case, at least not in the early stages of the thunderstorm outbreak.

Mansfield (1994) has recommended evaluating model performance by comparing model-derived PV patterns with WV imagery, because the dry intrusion air also brings down high PV from upper levels. An argument in favour of doing this is that the use of PV helps provide an understanding of the dynamical processes. However, it is possible to make a more rigorous comparison by comparing like with like, i.e. WV imagery with model-derived humidity patterns (Muller & Fuelberg (1990) and Schmetz & van de Berg (1994). To provide a rough and ready model product we have linearly averaged the model-derived relative humidities at 100 mb intervals over the layer 600 to 300 mb. The results for the present case are shown in Figure 7.

The model-derived forecast sequence of pseudo-WV imagery in Figure 7 clearly depicts the main bands of relative humidity along the cold front which trails from north of Scotland to the vicinity of Spain. Ahead of the cold front there is a narrow strip of moist air (coloured yellow and red); behind it there is a narrow strip of dry air (blue). Both are gently curved on the large scale but show relatively little tendency to wave on scales shorter than 1000 km. This situation prevailed throughout the period displayed.

The corresponding sequence of Meteosat WV imagery in Figure 8 shows the same two strips of moist and dry air. However, instead of remaining relatively straight as in the model, they display ripples with wavelength of about 700 km. One of them, over the Bay of Biscay. amplified strongly over the period. This is the system analysed in Sections 2 and 3. The first thunderstorms developed at 1430 and their tops account for the blobby appearance of the moist strip in the last two pictures in Figure 8. However, even before the outbreak of these thunderstorms, the amplification of the ripple in the WV imagery and the lack of any such effect in the corresponding model output (Figure 7) should in principle be sufficient to alert the forecaster of the failure of the model to represent an upper-level vortex.

5. Conclusions

We have presented a case study of frontal thunderstorms triggered by dry low-θ_w air overrunning and ascending above high-θ_w air ahead of a trailing cold frontal system. The case is analysed in terms of the split front model of a kata-cold front in which a dry intrusion overruns the warm conveyor belt to produce an upper cold front (UCF) that advances ahead of the surface cold front (SCF). The thunderstorms were triggered in the zone between the SCF and the UCF.

We have used Meteosat imagery to identify the SCF and UCF. Visible imagery is especially useful for identifying the SCF of a kata-cold front and WV imagery for identifying the UCF. Action replay of the WV imagery in a system-relative frame of reference has been found to be useful in drawing attention to the rotation of upper-level features of the imagery. This rotation indicated that the pattern of overrunning and ascent, and the ensuing

development of the thunderstorms, was due to the effects of a rather small-scale upper-level vortex (potential vorticity maximum). Forecast runs of the Meteorological Office's operational model failed to represent this vortex and its effects. Comparison of Meteosat WV image sequences with model-derived forecast sequences of pseudo-WV imagery is shown to be a useful means for identifying such a deficiency in model guidance. Research is required to determine how best to bogus the numerical model fields to take into account such information. In the meantime it is possible that, given the necessary user-friendly display facilities, a forecaster could obtain some benefit from the improved subjective understanding that such comparisons would provide.

We present only a single case study in this paper. However, we have evidence that it is not uncommon for thunderstorms to be associated with dry intrusions detected in the WV imagery. Research is continuing into the generality and utility of this relationship.

Acknowledgement

The Joint Centre for Mesoscale Meteorology is supported by the Meteorological Office and the Department of Meteorology, University of Reading.

References

Browning, K.A. (1993). Evolution of a mesoscale upper tropospheric vorticity maximum and comma cloud from a cloud-free two-dimensional potential vorticity anomaly. Q.J.R. Meteorol. Soc., 119: 883-906.

Browning, K.A. & Monk, G.A. (1982). A simple model for the synoptic analysis of cold fronts. Q.J.R. Meteorol. Soc., 108: 435-452.

Browning, K.A. & Roberts, N.M. (1994). Structure of a frontal cyclone. Q.J.R. Meteorol. Soc., 120: In press.

Browning, K.A., Bader, M.J., Waters, A.J., Young, M.V. & Monk, G.A. (1987). Application of satellite imagery in nowcasting and very short range forecasting. Meteorol. Mag., 116: 161-179.

Lee, A.C.L. (1989). Ground truth confirmation and theoretical limits of an experimental VLF arrival time difference lightning flash location system. Q.J.R. Meteorol. Soc., 115: 1147-1166.

Mansfield, D. (1994). The use of potential vorticity in forecasting cyclones: operational aspects. In 'The life cycles of extratropical cyclones. Vol III', Proc. International Symposium, 27 June - 1 July 1994, Bergen, 326-331.

Muller, B.M. & Fuelberg, H.E. (1990). A simulation and diagnostic study of water vapour image dry bands, Mon. Wea. Rev., 118: 705-722.

Schmetz, J. & van de Berg, L. (1994). Upper tropospheric humidity observations from Meteosat compared with short-term forecast fields, Geophys. Res. Letters, 21: 573-576.

Weldon, R.B. & Holmes, S. J. (1991). Water vapor imagery, interpretation and applications to weather analysis and forecasting. NOAA Tech. Report NESDIS 57, 213pp.

Young, M.V., Monk, G.A. & Browning, K.A. (1987). Interpretation of satellite imagery of a rapidly deepening cyclone. Q.J.R. Meteorol. Soc., 113: 1089-1115.

Figure captions

Figure 1. Analyses for 1200 UTC, 27 July 1994. (a) Surface analysis from the Central Forecasting Office of the Meteorological Office. (b) Wet-bulb potential temperature analyses (solid lines for 900 mb; dashed lines for 500 mb) derived from the operational Meteorological Office Unified Model.

Figure 2. Meteosat imagery for 1300 UTC, 27 July 1994, showing the portion of the cold front west of the Bay of Biscay: (a) visible, (b) infra-red, and (c) water vapour channel. Colour code is as follows: (a) Clouds, in order of diminishing brightness - red, yellow and green; least bright clouds and cloud-free areas, blue. (b) Cloud tops colder than -35, -28,-21, -14, -7, 0 and 7 C are shown red, orange, yellow, light green, medium green, dark green, and bright blue, respectively. Cloud tops and earth surfaces warmer than 7, 14 and 21 C are medium, dark and very dark blue, respectively. (c) Moist areas in order of diminishing humidity - red, yellow, and green; driest areas, dark blue.

Figure 3. Frontal analyses for (a) 0630, (b) 1230 and (c) 1830 UTC, 27 July 1994, derived from Meteosat imagery as explained in text. The front with conventional symbols is the surface cold front (SCF). The scalloped curve represents the upper cold front (UCF), following the scheme proposed by Browning and Monk (1982). The axis of the 'moist head' has been derived from the WV imagery, and the S-shaped curve corresponds to the boundary of part of the associated bright blue area. The large dot in the middle of the S-shaped curve turns out to be a centre of rotation (see text).

Figure 4. Successive positions for (a) 1500, (b) 1600 and (c) 1700 UTC, 27 July 1994, of the potentially unstable region between the surface cold front (SCF) and upper cold front (UCF). Crosses show the locations of sferics recorded within $\pm$30 minutes of each hour.

Figure 5. Meteosat infra-red imagery for (a) 1700 and (b) 2000 UTC, 27 July 1994, with frontal analyses superimposed. Cloud top temperature colour code is same as for Figure 2(b). The letters A and B refer to two distinct areas of thunderstorms discussed in the text. The SCF and UCF are drawn using the same convention as in Figure 3. The dashed line marks the quasi-stationary western boundary of high-θ_w air streaming downwind from the Spanish mainland.

Figure 6. Successive positions of (a) the moist head, as explained in caption to Figure 3, (b) the upper cold front (UCF), plotted relative to the position of the moist head at 1830 UTC, and (c) the thick anvil cloud from Thunderstorm Area B, again plotted relative to the position of the moist head.

Figure 7. Sequences of forecast pseudo - WV images for (a) 0600, (b) 1200, and (c) 1800 UTC, 27 April, and (d) 0000 UTC, 28 April 1994, derived as explained in the text from the midnight run (26/27 July) of the Meteorological Offices' operational Unified Model.

Figure 8. Sequence of Meteosat WV images for (a) 0630, (b) 1230, and (c) 1830 UTC, 27 April, and (d) 0030 UTC, 28 April 1994, for comparison with Figure. 7. Colour code is the same as in Figure 2(c).

Fig 1(a)

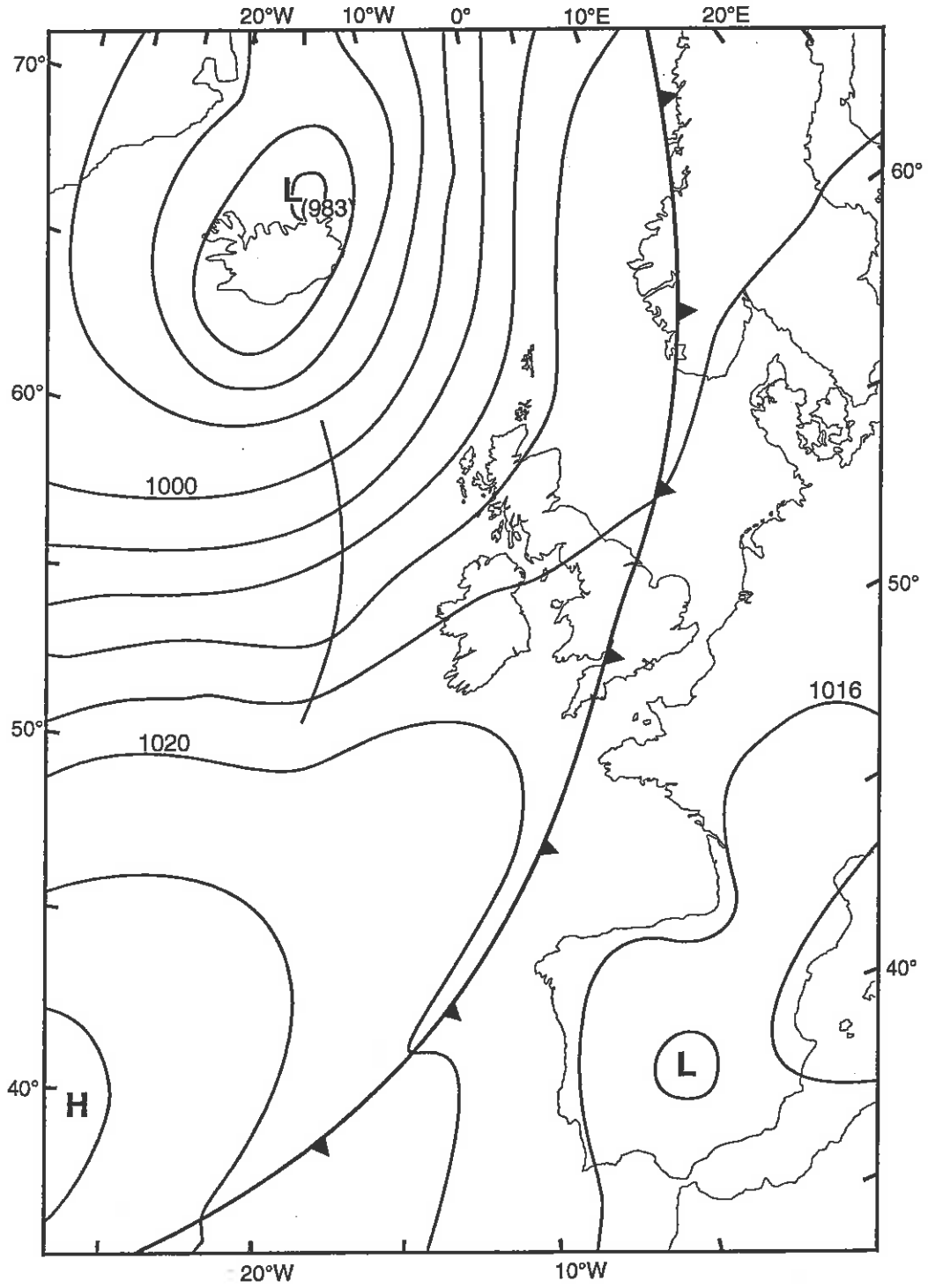

Fig 1(b)

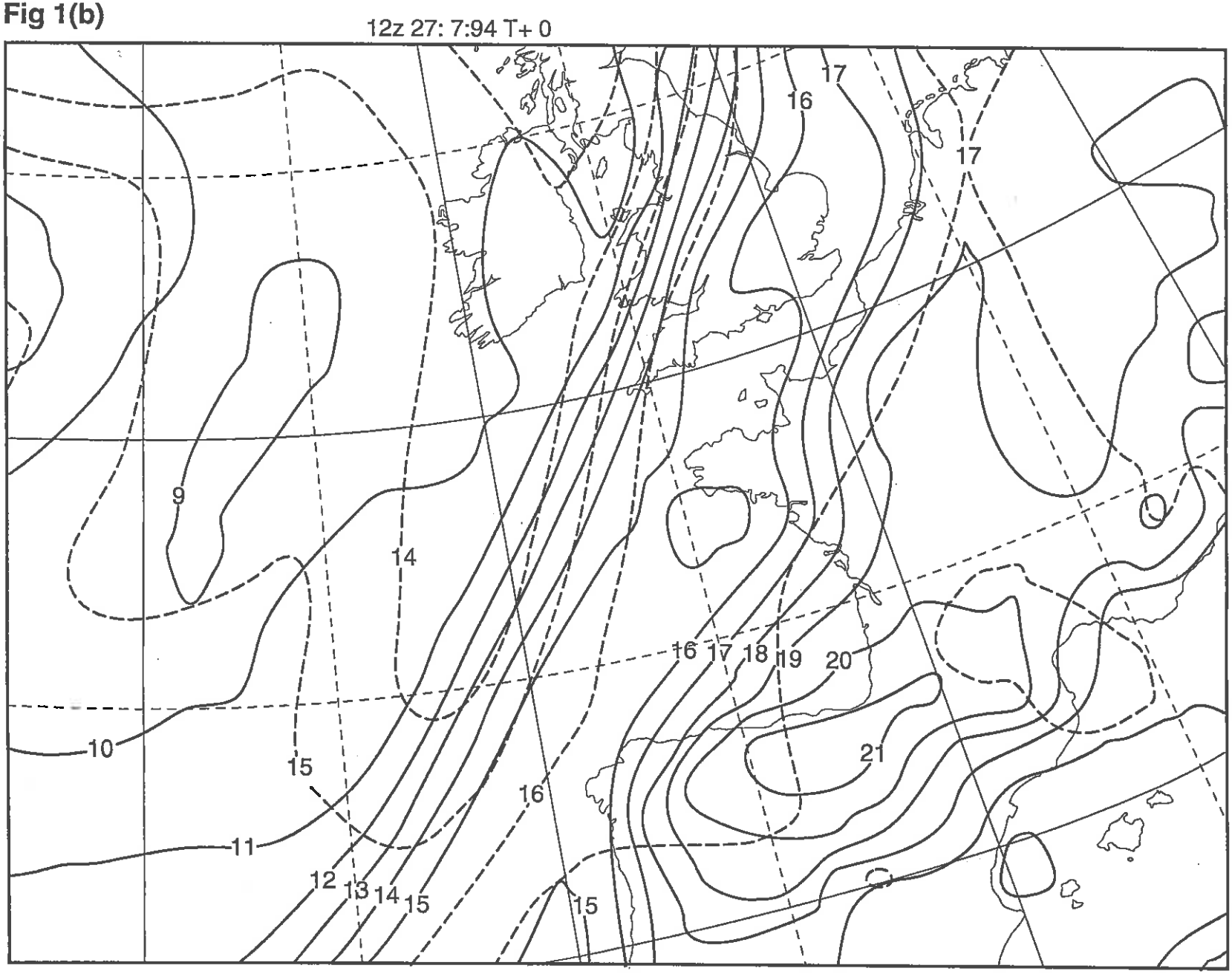

Fig. 2.

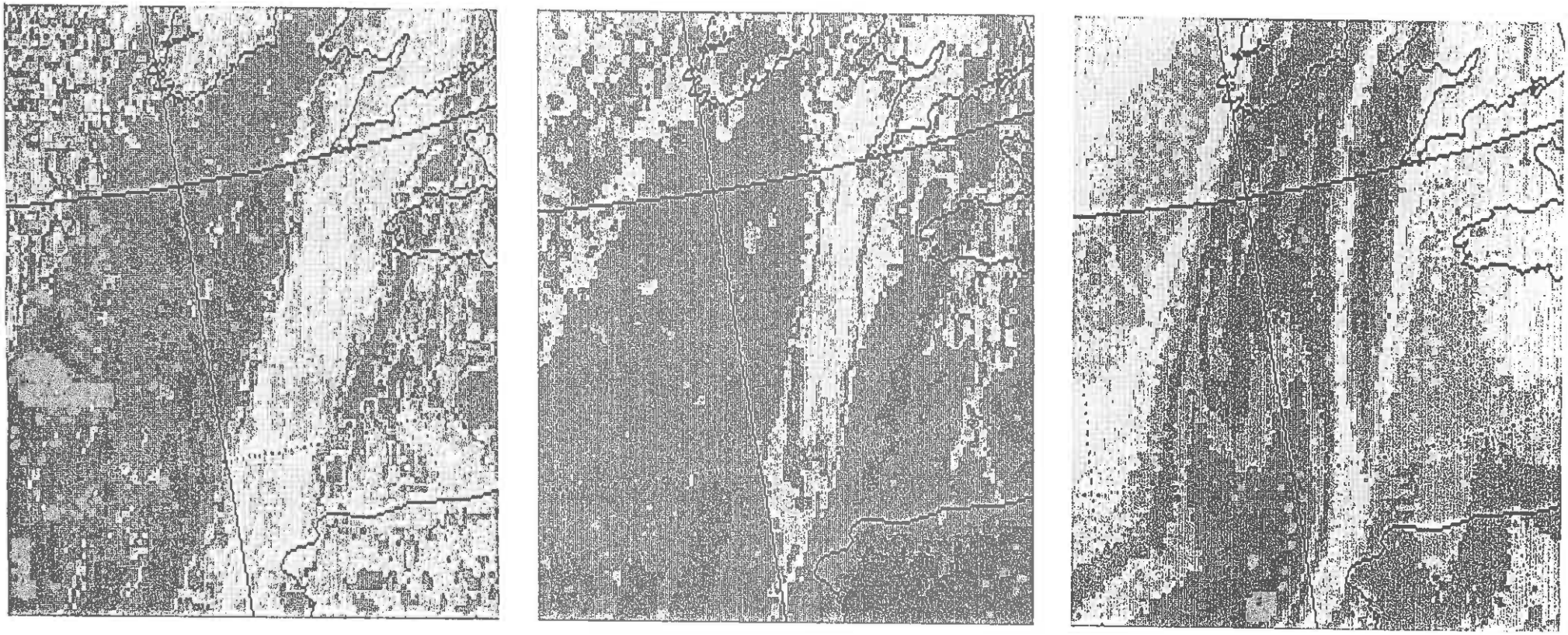

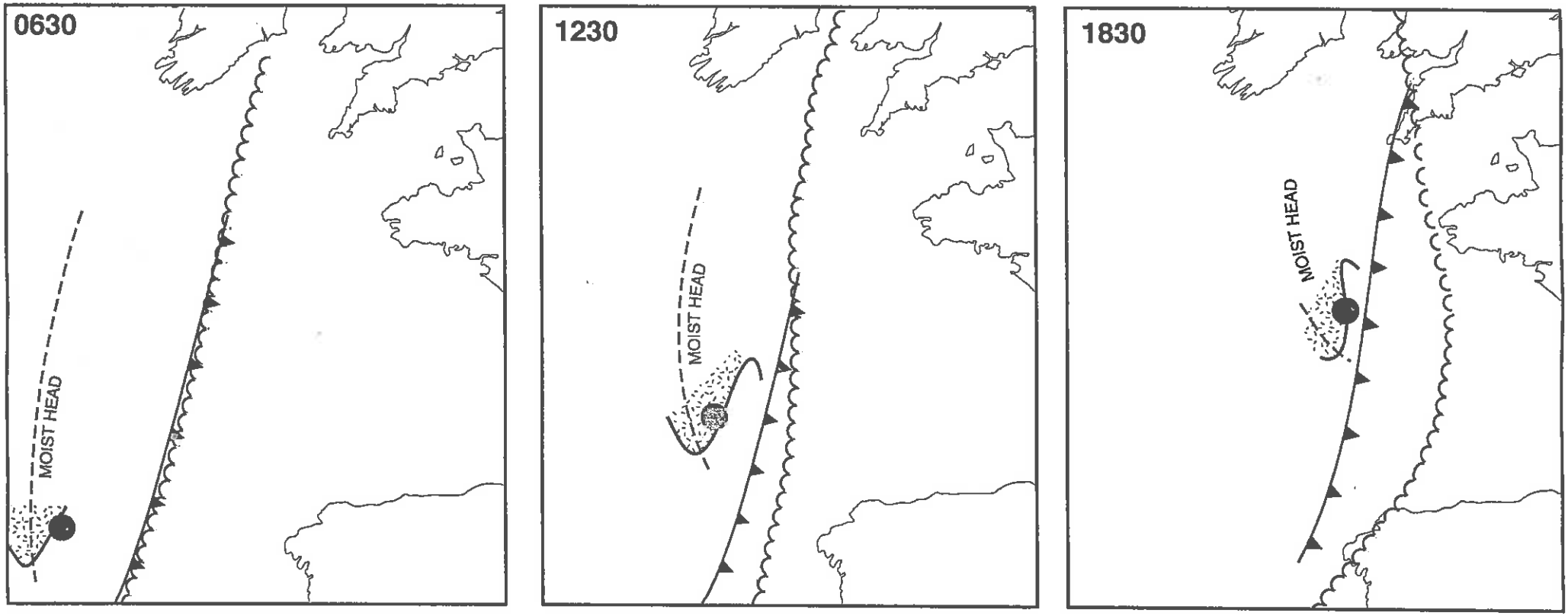

Fig 3

Fig. 4.

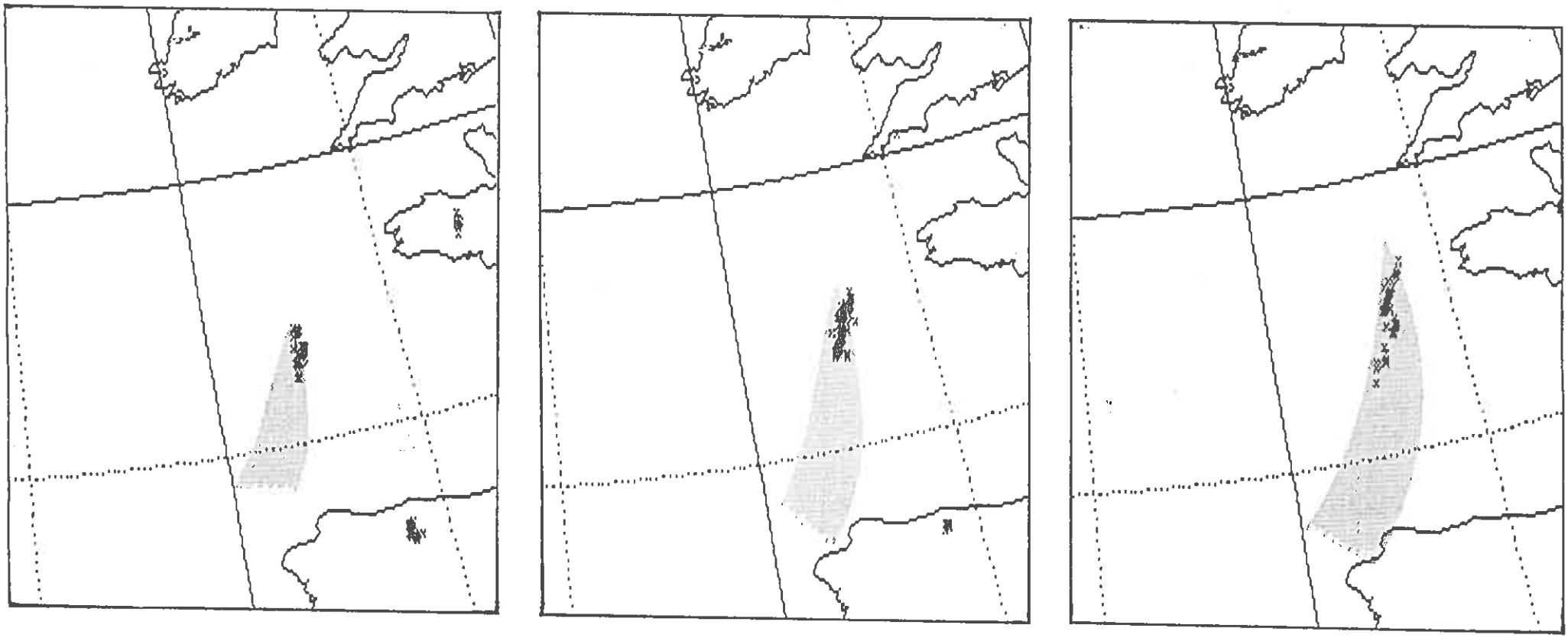

Fig. 5.

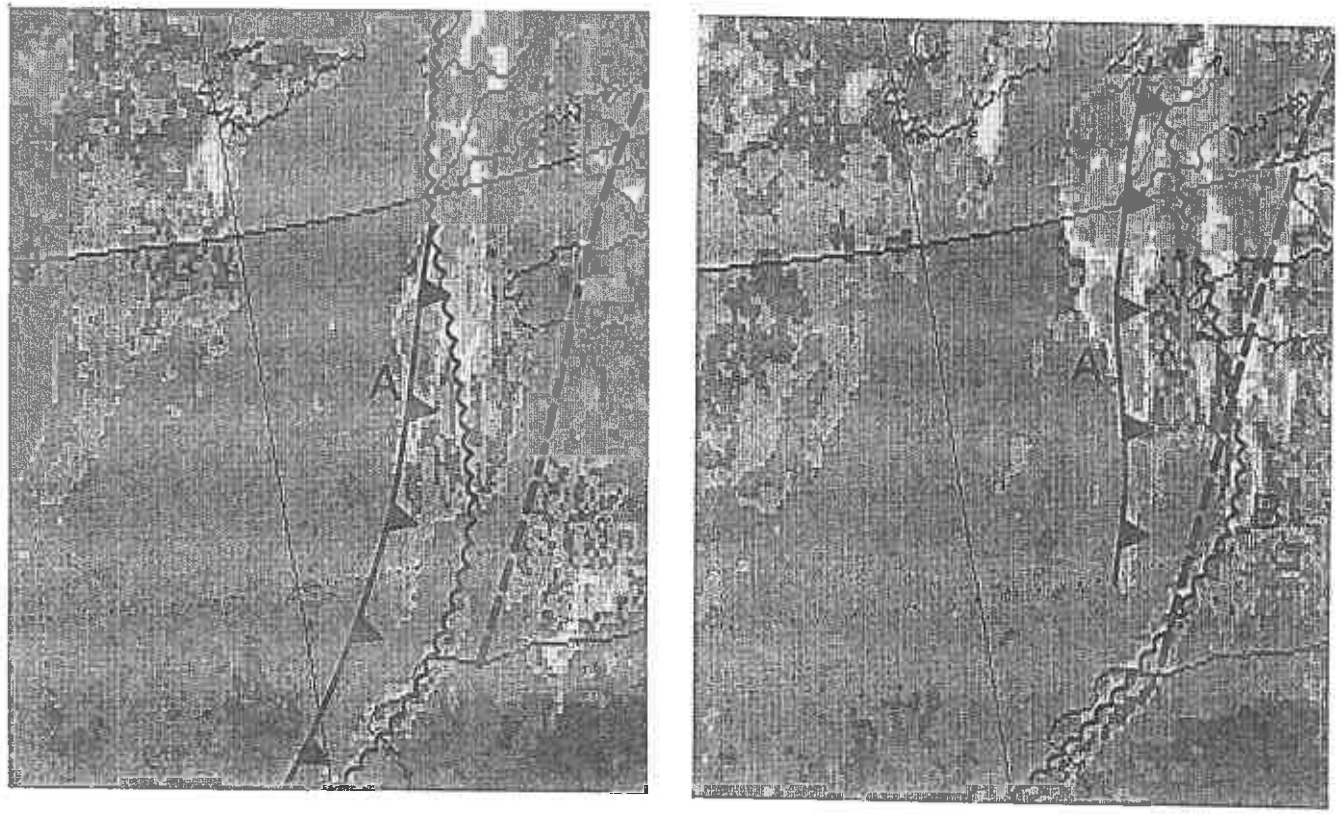

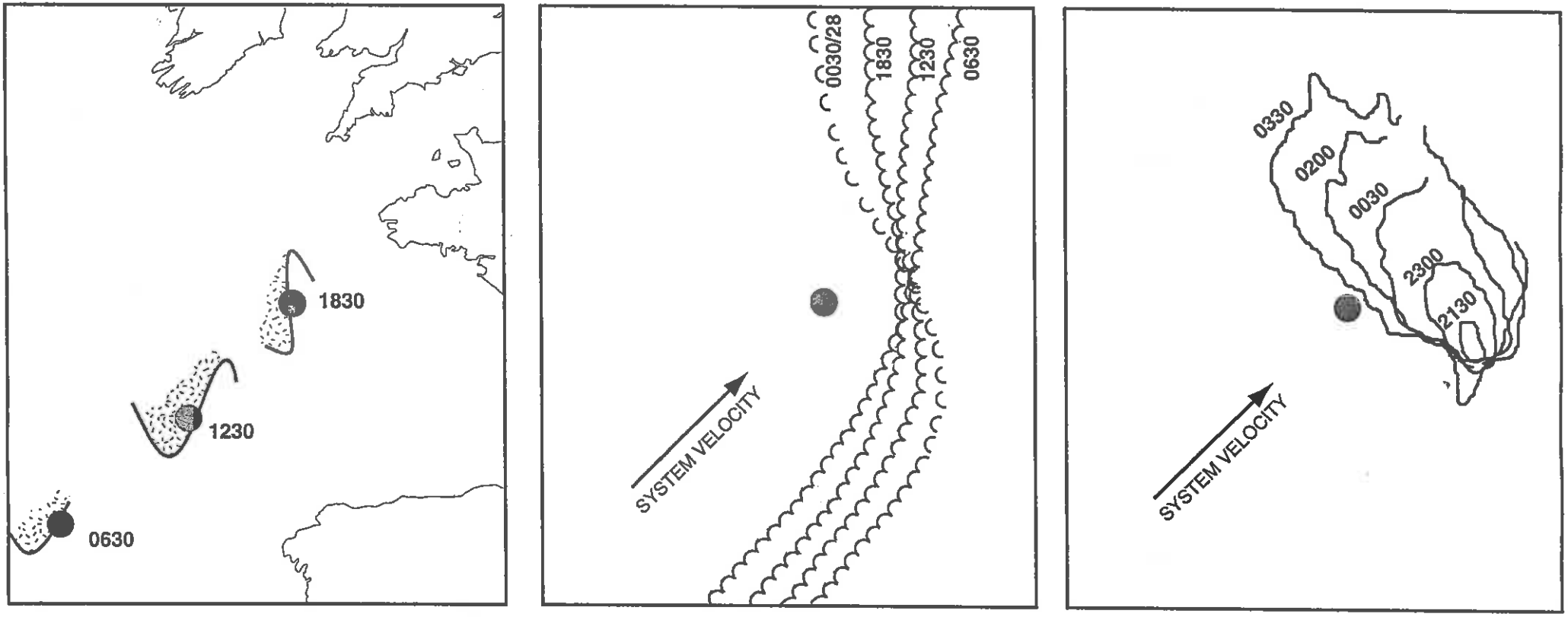
1830
1230
0630
0030/28
1830
1230
0630
SYSTEM VELOCITY
0330
0200
0030
2300
2130
SYSTEM VELOCITY

Fig 6

Fig. 7.

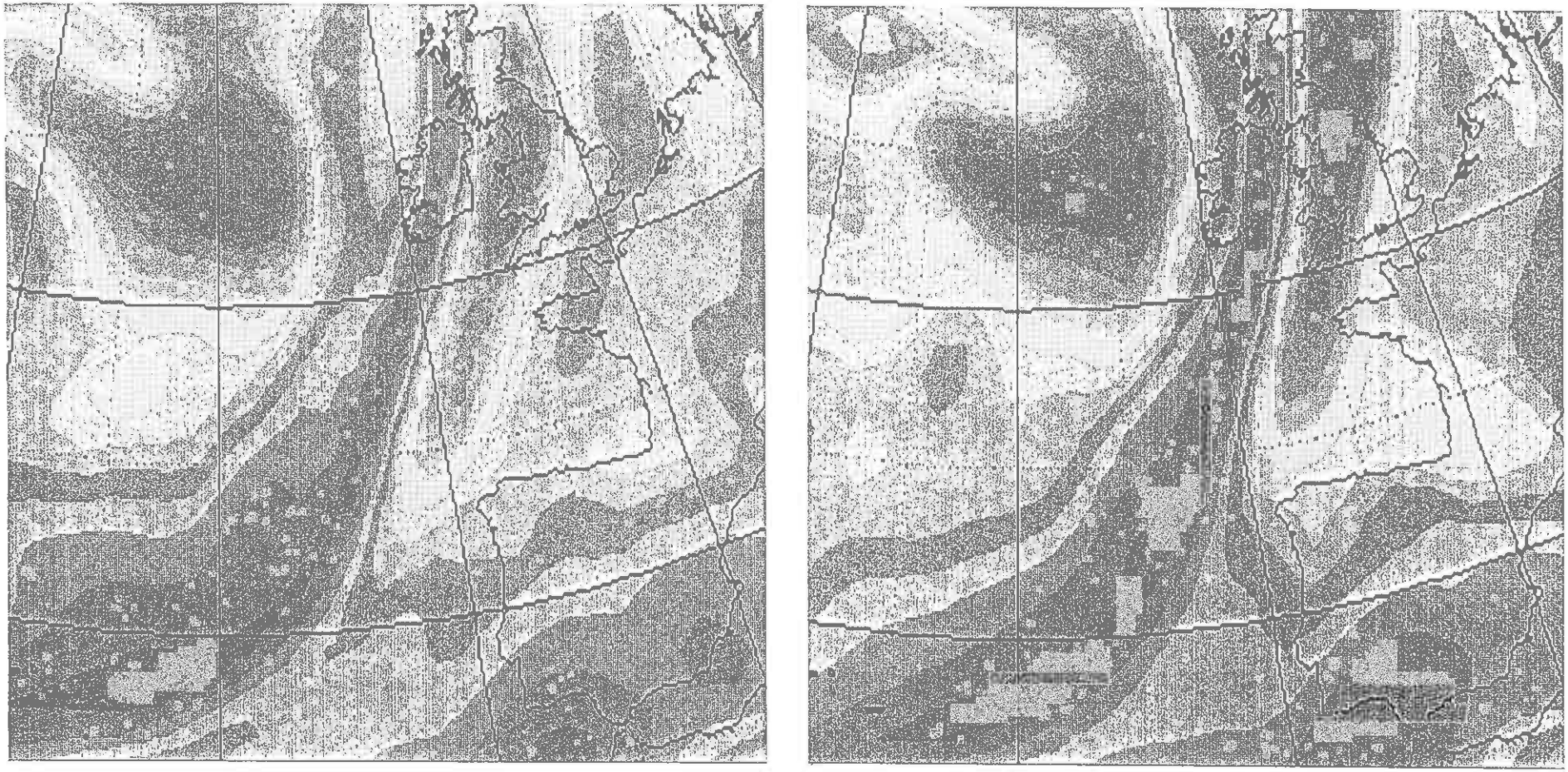

(a) (b)

Fig. 7.

(c)

(d)

Fig. 8.

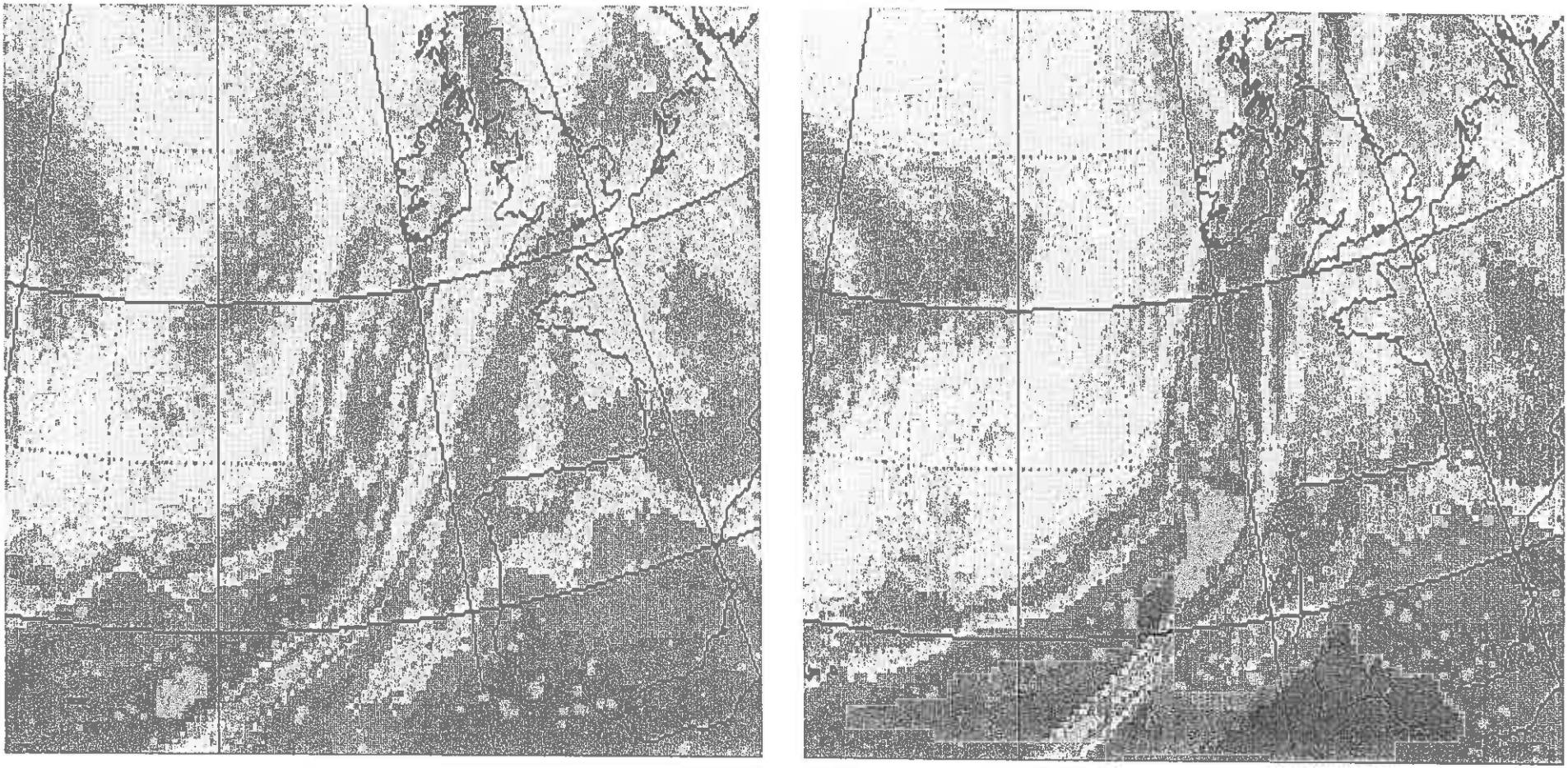

(a)

(b)

Fig. 8.

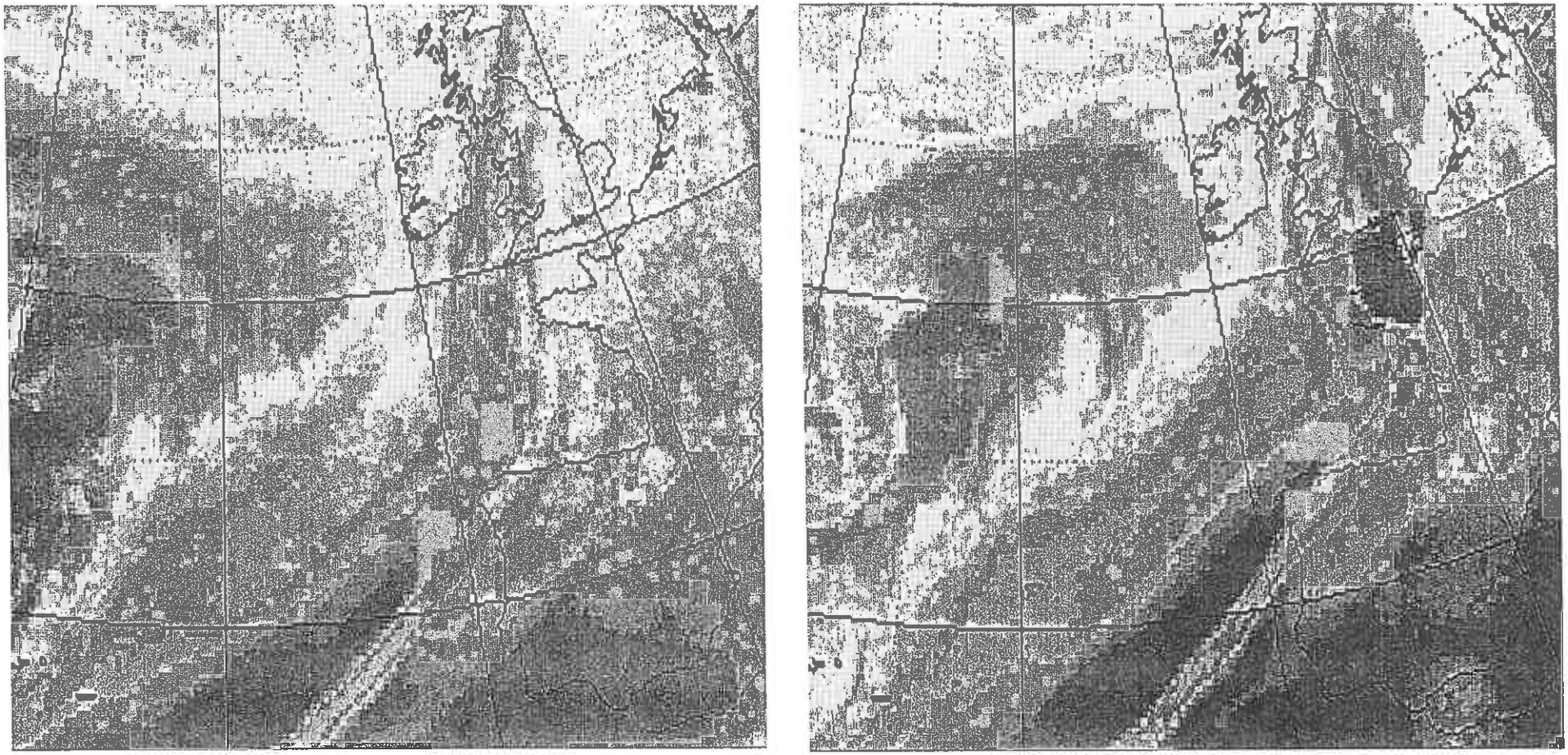

(c)

(d)

Version dated 28 November 1994

Use of satellite imagery to diagnose events leading to frontal thunderstorms: part II of a case study

K A Browning and N M Roberts
Joint Centre for Mesoscale Meteorology, Harry Pitt Building,
University of Reading, Whiteknights Road, PO Box 240
Reading RG6 2FN, UK

Abstract

Convective and mesoscale processes can be diagnosed in some detail by careful scrutiny of high-resolution satellite imagery. An example is presented in which lines of convergence within warm, moist, low-level air created a series of very straight rope-like clouds whose smooth texture in polar orbiting satellite imagery indicated that they were capped by a stable lid. The moist air deepened with time until the lid was penetrated and deep convection was observed to break out. The rope-like clouds occurred near the leading edge of a so-called dry intrusion and they are believed to have been associated with the kind of multiple cold frontal structure often encountered in such regions.

1. Introduction: an informative pair of NOAA cloud images

The motivation for this short article is twofold. First, it is to illustrate by means of a case study how the close inspection of satellite imagery can provide a forecaster with an understanding of what is happening on the mesoscale. Second, it is to use the analysis of the specific event to add to our general understanding of the way in which clusters of frontal thunderstorms may be triggered by overrunning cold fronts.

The inspiration for this study is provided by the high-resolution visible and infra-red NOAA images in Figures 1(a) & (b). The band of clouds extending from the bottom left corner of Figure 1 to the top right corner was situated in the Bay of Biscay and was associated with a cold front as shown in Figure 2. The images in Figure 1 are interpreted in the context of the analysis of a time series of lower-resolution Meteosat images for the same

occasion; broader-scale aspects of these images have been analysed in an earlier article in this journal by Browning and Roberts (1994) (hereafter referred to as BR) and we draw upon some of their findings to provide the context for the more detailed analyses presented here.

The highlights of Figure 1 are identified in Figure 3(a). They are:

(i) A small cluster of cumulonimbus in the centre of the frame, identifiable from the cold bright tops with sharp knobbly edges. (This is the outbreak of storms referred to in BR as Storm Area A).

(ii) A band of cirrostratus at the northern end, with traces of embedded convection. The cloud-top temperatures of the cirrostratus are mainly in the range -30 to -40C.

(iii) Several rope-like clouds extending into (i) and (ii). The main rope clouds, A_1, A_2 and A_3, are spaced about 40km apart and were trackable within the Meteosat imagery from 12 to 18 UTC. A_1 extended into the cirrostratus. A_2 and A_3 extended into the cumulonimbus clouds. Each of the three rope clouds was about 10km wide and up to 300km long. Their cloud top temperatures were mainly in the range 0C to -20C and the tops had a notably smooth appearance. The tops of these rope clouds were higher than those in the usual kind of rope clouds described in the literature (eg Scorer 1986). Moreover they were not surrounded by cloudless skies in the way that makes many ordinary rope clouds stand out so clearly.

As shown by the tephigram later in this article, the atmosphere in this region was characterised by dry air with low wet-bulb potential temperature (θ_w) at upper levels and moist high-θ_w air at low levels. According to BR this case was a split cold front (as defined

by Browning and Monk 1982), in which the low-θ_w air overran the high-θ_w air to give an upper cold front (UCF) ahead of the surface cold front (SCF). Figure 3(a) shows the positions of the UCF and SCF as inferred in BR from an analysis of the Meteosat imagery. Note that, although the cirrostratus is ahead of the UCF, the cumulonimbus and rope clouds are behind the UCF but ahead of the SCF. The region between a SCF and UCF is generally characterised by potential instability according to the split front model of Browning and Monk (1982) and, given enough lifting and deepening of the moist layer, thunderstorms may develop, as indeed happened in the present case.

Figure 3(b) shows sections across the axes of the rope-like clouds inferred from the infra-red imagery. It shows the variations in the depth of the cloudy lower-tropospheric air within which the rope clouds were embedded. The tops of the rope clouds in Figure 1 became colder (higher) with distance along their axes towards the north and, in the case of rope clouds A_2 and A_3, they erupted into cumulonimbus at their northern end. This, along with the smooth appearance of the rope clouds, suggests (a) that the rope clouds were due to lines of lower-tropospheric convergence, initially capped by a stable layer or lid, and (b) that the lid was broken when subjected to sufficient lifting, thereby allowing buoyant ascent of low-level air with high θ_w into the upper troposphere. This interpretation is confirmed and quantified in Section 3 of this article by reference to operational numerical weather prediction model output. But first in Section 2, we extend our interpretation by looking more closely at the evolution of the rope clouds and associated cumulonimbus as seen in the geostationary satellite imagery. In Section 4 we shall draw attention to similarities with another recent study which suggests that the rope clouds may have been generated by a multiply-segmented

cold frontal structure near the leading edge of the intrusion of dry low-θ_w air, the so-called dry intrusion.

2. Evolution of the rope-like cloud systems as seen in Meteosat imagery

Hourly positions of the axis of rope cloud A_2, derived from Meteosat IR imagery, are plotted in Figure 4. First signs of cloud tops colder than -25C are seen at the northern end of the rope cloud at 15 UTC, 3 hours after the appearance of the rope cloud. Sferics recorded by the Met Office ATD system were found to be situated within the envelope of the -25C tops, the first sferic being recorded just before 15 UTC. Over the next 2 hours the thunderstorm top and associated anvil grew steadily in area.

An indication of the vertical structure of rope cloud A_2 is provided by Figure 5 which depicts the cloud top temperature and inferred height along its axis. The solid line emphasised with hatching shows the structure at nominal time 16 UTC corresponding roughly to Figures 1 and 2. The earlier evolution of the cloud tops is depicted by the dashed and dotted curves. For the most part the height of the rope cloud increased with time and distance to the north, from about 1 to 6km. The thunderstorm that developed at its northern end had a top that rose a further two kilometres, from 6 to 8km, between 14 and 15 UTC. Evidently the lid that was constraining the rope cloud had to be lifted to above 6km before it could be penetrated by convective updraughts. (The locally lower tops within a few tens of kilometres just south of the storm are presumably due to compensating subsidence in their wake.)

A similar analysis is shown in Figure 6 for rope cloud A_1. This rope cloud was lifted to upper levels without any significant convection breaking out. At its northern end, where according to Figure 1 it evolved from a smooth-edged rope into ragged cirrostratus, indicating the eradication of the lid, its height was 7km. Although this was the level where the stable lid would have been eliminated, presumably here at the leading edge of the colder air aloft there was insufficient potential instability to promote vigorous convection.

Another similar analysis, for rope cloud A_3 (not shown), suggests that farther back into the advancing cold air the lid was not as strong as it was for rope clouds A_1 and A_2. Thus, whereas the tops of rope clouds A_1 and A_2 reached 6km before losing the smooth appearance, in the case of rope cloud A_3 the deep cumulonimbus convection erupted when it was lifted to only 4km.

3. Consistency of the image interpretation with model output

In this section we interpret the thermodynamic structure of the evolving atmosphere in the vicinity of the thunderstorm outbreak in terms of a vertical sounding derived from the Met Office's operational limited area model. It was shown in BR that this model reproduced the broad features of the situation, but that it underestimated the effects of a small upper-level vortex both in creating potential instability through the overrunning of low-θ_w over high-θ_w air and in creating sufficient large-scale ascent to release the instability. In order to compensate for the model's failure to advect low-θ_w air at upper levels sufficiently far ahead of the position of the SCF, we have generated a composite sounding (Figure 7). In this we have employed the model's original sounding below 900mb, but at all higher levels we have

used the model sounding derived from a location about 150km upwind to compensate for the failure of the model to represent the overrunning of dry air aloft. To compensate for the model's failure to produce sufficient uplift we have generated additional temperature curves in Figure 7 to correspond to 50 and 70mb of extra lifting.

One of the key features of Figure 7 is the stable lid characterised by dry air with θ = 32C. Further support for the existence of this lid is given by the 11 UTC sounding at Corunna (NW tip of Spain). Although this is a little too far south of the main region of interest, nevertheless it too shows a lid with θ = 32C. It was at 800mb rather than 700mb as in the original model sounding, consistent with the smaller degree of uplift farther away from the vortex centre.

Our interpretation of the model sounding may be summarized as follows. The lid in these soundings marks the upper limit of a convective boundary layer which was deepening with time under the influence of the upper level vortex discussed in BR. Until the boundary layer had deepened to 4km the convection would have been constrained by the lid and tops of clouds would have retained the rather smooth appearance of the rope clouds seen in Figure 1. The deep cumulonimbus convection would have been expected to erupt once the lid was lifted above 630mb (4km). At this stage Figure 7 suggests that the convection would have broken through to a new equilibrium level of about 400mb (7km). To the extent that the model may have underestimated the strength of the lid, even greater lifting would have been required to break through the lid and the resulting convectively available potential energy would also have been greater. This interpretation is reasonably consistent with the analysis

of the imagery in Section 2 which shows that the deep thunderstorms developed after the rope cloud tops reached 6km in the case of A_2 and 4km in the case of A_3.

We have argued in terms of large-scale ascent lifting the stable lid and deepening the boundary-layer convection until such time as the air was able to penetrate the lid and create the thunderstorms. This is of course only part of the story because the large-scale ascent was being modulated by the pattern of mesoscale convergence responsible for the series of rope clouds. The difference in cloud-top height between the axes of the rope clouds and the troughs between them was typically 1.5km (see Figure 3(b)). Such differential lifting is important for the generation of thunderstorms because it provides the means for triggering deep convection locally whilst restraining it elsewhere.

4. A possible cause of the rope-like clouds

We believe that the mesoscale convergence lines responsible for the multiple rope clouds may have been due to a multiple cold frontal structure, although we do not have the detailed evidence to prove it. The basis for our belief is the resemblance of these thin cloud lines to those analysed in detail in the FRONTS 92 experiment by Browning et al (1995). In FRONTS 92 a large number of dropwindsondes were released in an observational study of a developing cyclone. Part of the study focussed on the fine-scale structure of the cold frontal region overrun by dry-intrusion air. It showed that mesoscale instabilities at the leading edge of the dry intrusion led to a series of closely-spaced incursions of dry air with low θ_w and high vorticity, which impacted the top of a moist boundary layer and created a series of weak kata-cold frontal cloud lines. In the FRONTS 92 study the cloud lines were

not as deep, nor were they as smooth as in this case; however, their multiple structure and their position with respect to an upper-level vortex and an encroaching dry intrusion were similar.

5. Concluding remarks

We have shown that the cloud images in Figure 1 are consistent with the following:

- Thunderstorms broke out at the northern end of a series of rope-like clouds.

- The rope clouds were associated with narrow bands of lower-tropospheric convergence. It is hypothesized that these convergence lines were multiple cold fronts driven by mesoscale instabilities within an overrunning dry intrusion characterised by low θ_w.

- The smoothness of the tops of the rope clouds, and the suppression of deep convection until the tops of the rope clouds were lifted into the middle troposphere, indicates that the high-θ_w air in the lower troposphere was capped by a stable lid.

- The breaking of the lid and the ensuing storms were the result of large-scale ascent associated with an upper-level vortex, modulated strongly by the mesoscale pattern of vertical motion responsible for the individual rope clouds.

The value of geostationary satellite imagery for diagnosing what is happening on the convective and mesoscale has long been appreciated (eg Purdom 1982). However, it is important to have not only frequent images but also sufficiently high spatial resolution to resolve fine details of the cloud structure, eg to be able to distinguish the smooth texture of a rope cloud as an indicator of the existence of a stable lid. The resolution of the current generation of Meteosat imagery is inadequate for this purpose and in this study we had to make use of a single pair of sun-synchronous satellite images which by luck captured the most interesting stage in the evolution of the clouds. In Europe we look forward to the availability of images with improved resolution from Meteosat Second Generation.

We have deliberately chosen to present in this paper a clear-cut case, away from the complicating effects of topography. It has to be said, however, that the multiplicity of interacting small-scale effects, combined with the frequently poor visibility over mainland Europe, often prevents such simple interpretations. But, with the planned improvements in the resolution of Meteosat imagery, the forecaster's ability to make useful interpretations is also likely to improve, even in the more complex situations. This is where the role of the human will become paramount in the future man-machine mix.

Acknowledgement

The Joint Centre for Mesoscale Meteorology is supported by the Meteorological Office and the Department of Meteorology, University of Reading.

References

Browning, K.A. and Monk, G.A. (1982): A simple model for the synoptic analysis of cold fronts, *Q.J.R. Meteorol. Soc.*, 108: 435-452

Browning, K.A. and Roberts, N.M. (1994): Use of satellite imagery to diagnose events leading to frontal thunderstorms: a case study. *Met. Apps*. Submitted

Browning, K.A., Clough, S.A., Davitt, C.S.A., Roberts, N.M., Hewson, T.D. and Healey, P.G.W (1995): Observations of the mesoscale sub-structure in the cold air of a developing frontal cyclone. *Q.J.R. Meteorol. Soc.*, 121, Submitted

Purdom, J.F.W. (1982): Subjective interpretation of geostationary satellite data for nowcasting. Chap 3.1 in *Nowcasting*, Ed, K.A. Browning, Academic Press Inc, pp 149 - 166

Scorer, R.S. (1986): Cloud investigation by satellite. Ellis Horwood, 314 pp.

Figure Legends

Figure 1. NOAA satellite pictures for 1529 UTC, 27 July 1994: (a) visible, (b) infra-red. The overall cloud system of interest extends from the bottom left to top right. See Figure 2 for location of the images. Courtesy of Univ of Dundee.

Figure 2. Surface analysis for 12 UTC, 27 July 1994 from the Central Forecasting Office of the Meteorological Office. Also shown, over the Bay of Biscay, is the location of the satellite pictures in Figure 1 together with the 16 UTC position of the surface cold front.

Figure 3(a) Sketch showing salient features of Figure 1 and other information as discussed in the text.

Figure 3(b) Height of cloud tops along the cross-sections XX (solid curve) and X^1X^1 (dotted curve) in Figure 3(a), and other features discussed in the text, derived from Meteosat imagery at 16 UTC. The cross section XX is 70km north of X^1X^1.

Figure 4. Hourly tracings of the axes of rope cloud A_2 from 12 to 18 UTC, 27 July 1994, derived from Meteosat infra-red imagery. The shaded areas from 15 UTC onwards represent cloud tops colder than -25C associated with the thunderstorm that developed at the end of the rope cloud. The frame corresponds to the area shown in Figure 1.

Figure 5. Height (and temperature) of cloud top along axis of rope cloud A_2 at hourly intervals as derived from Meteosat infra-red imagery. The solid line emphasized by hatched shading represents the rope cloud at approximately the time of the NOAA pictures in Figure 1. (As with all other Meteosat times quoted in this article, the true time is about 10 minutes earlier than the nominal time.) Also shown by dotted, short-dash and long-dash lines, respectively, are the heights of rope cloud A_2 at nominal hours 13, 14 and 15 UTC. The origin of successive hourly tracings is displaced with the velocity of the cloud features that developed into the thunderstorm (14 m s^{-1} from 210°).

Figure 6. Same as Figure 5 but for rope cloud A_1.

Figure 7. Model-derived sounding for 15 UTC, 27 July 1994 for location S in Figure 3(a). Temperature and dew point curves for the sounding without additional lifting imposed are shown dotted. Winds are plotted on the right; thick, long and short barbs represent 25, 5 and 2.5 m s^{-1}, respectively. Temperature curves with 50 and 70mb extra lifting are shown dashed and solid, respectively. The 'positive area' indicating buoyant ascent for parcels with θ_w = 15C in the presence of 70mb lifting, is shown hatched. Also shown (dotted curve) is a portion of the temperature profile from the 11 UTC Corunna radiosonde. Note the presence of a stable lid with θ = 32C on all the profiles except for the one with maximum lifting.

Fig 1(a)

TOP

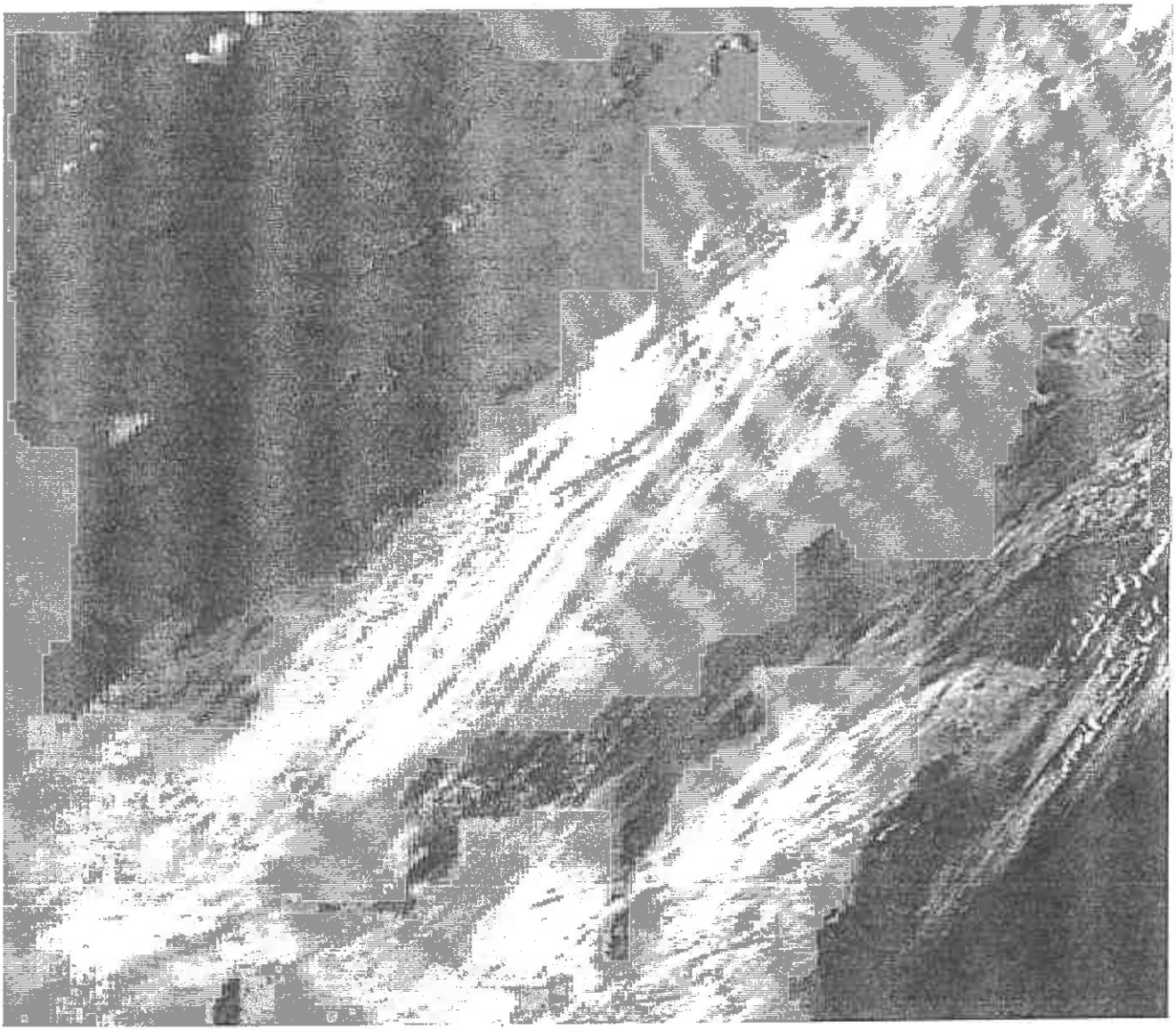

Fig 1(b)

TOP

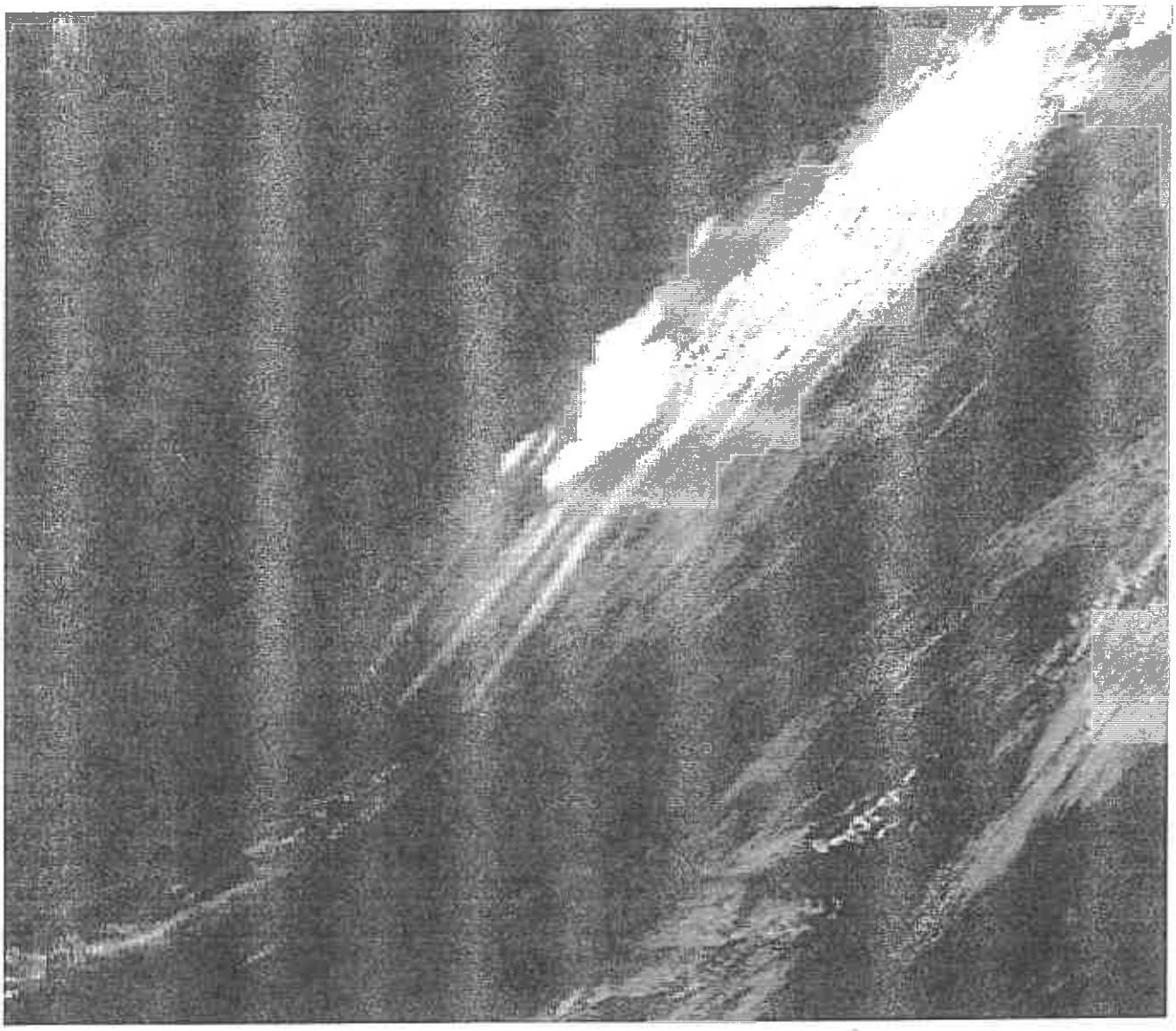

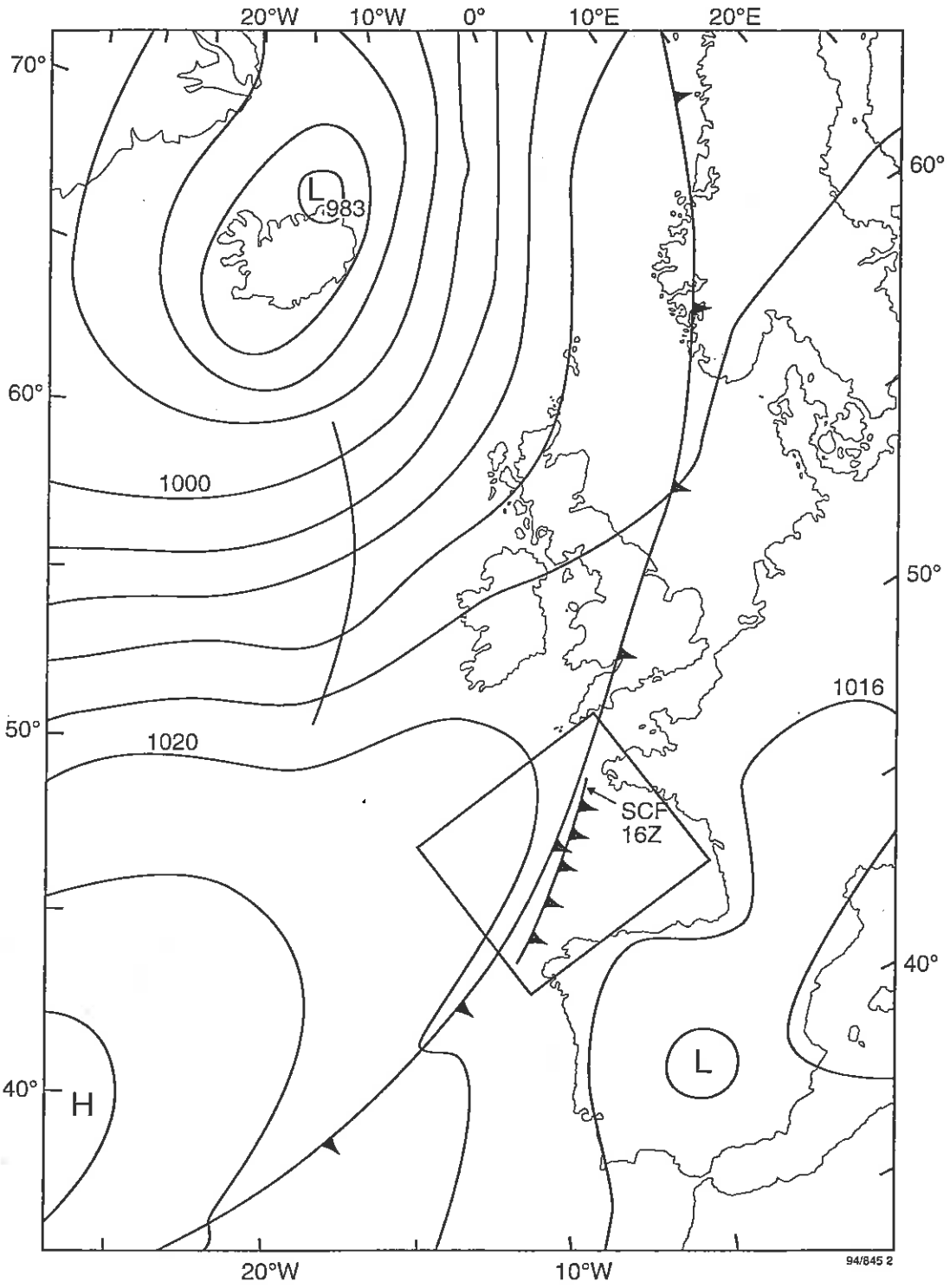
20°W
10°W
0°
10°E
20°E
70°
60°
50°
40°
L
983
1000
1020
1016
SCF
16Z
H
L
94/845 2

Fig 2

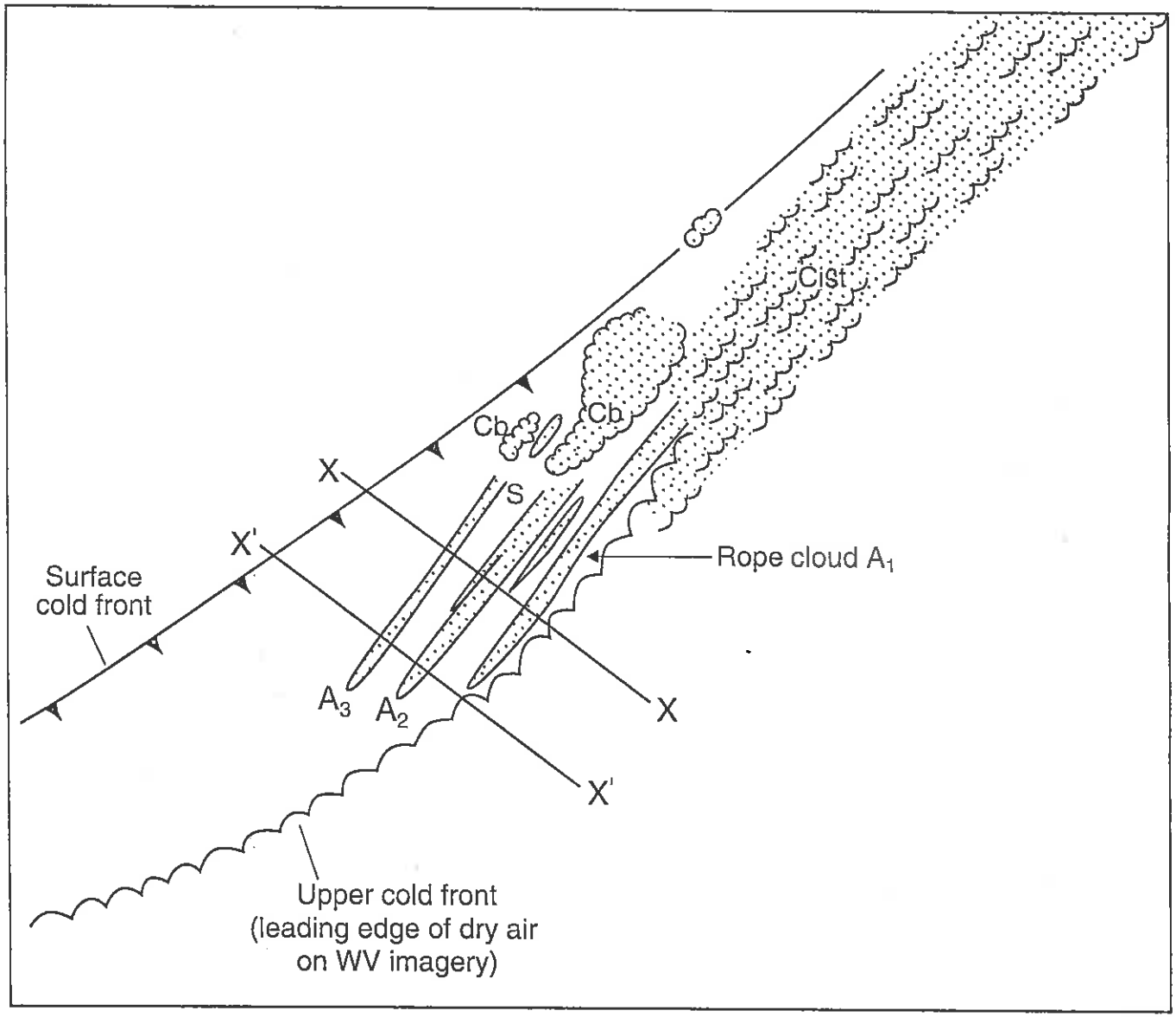
Cist
Cb
Cb
X
X'
S
Surface
cold front
Rope cloud A_1
A_3
A_2
X
X'
Upper cold front
(leading edge of dry air
on WV imagery)
94/845 3a

Fig 3(a)

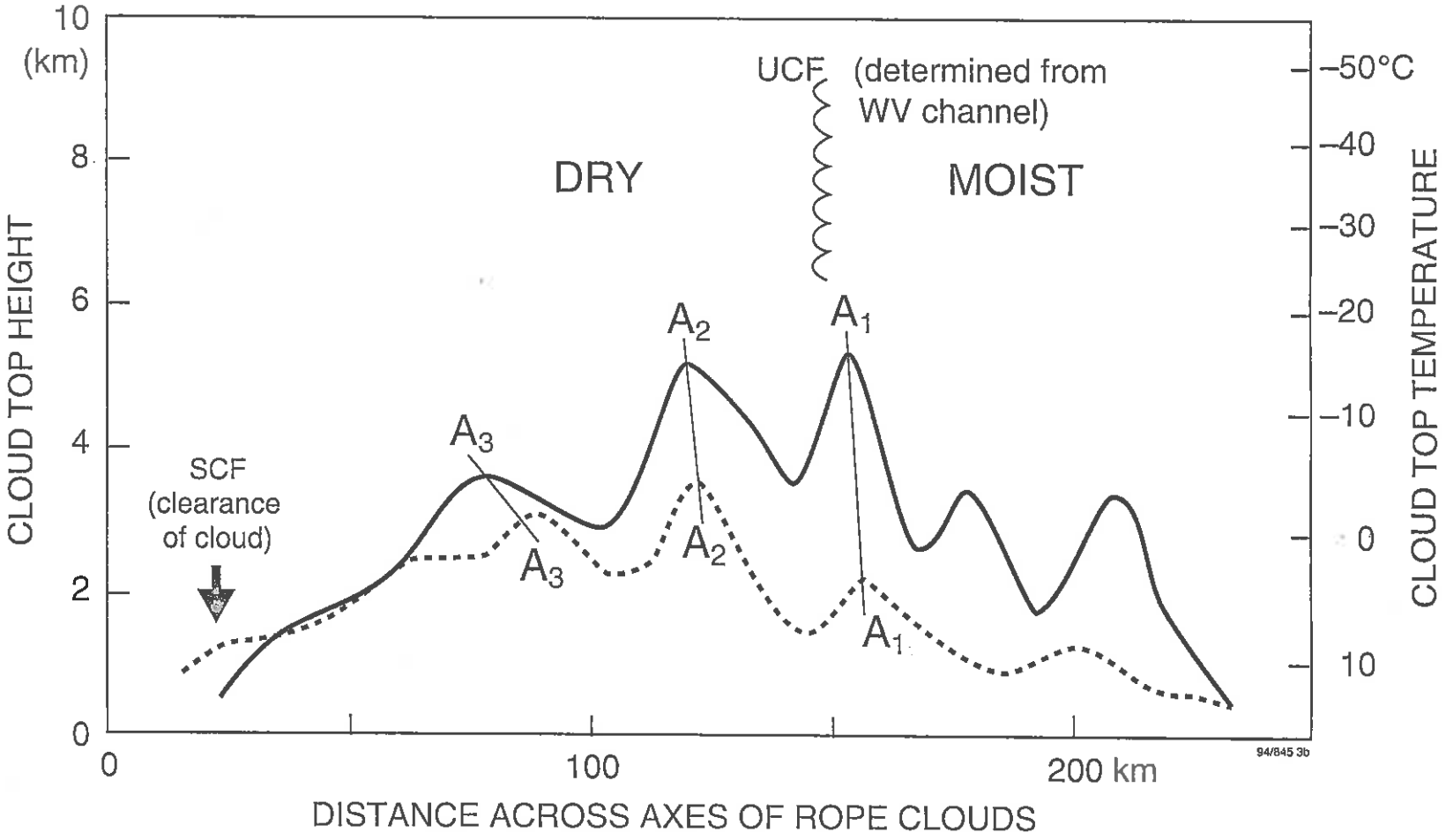
10
(km)
8
6
4
2
0
CLOUD TOP HEIGHT
UCF (determined from
WV channel)
DRY
MOIST
A2
A1
A3
SCF
(clearance
of cloud)
A3
A2
A1
0
100
200 km
DISTANCE ACROSS AXES OF ROPE CLOUDS
94/645 3b
–50°C
–40
–30
–20
–10
0
10
CLOUD TOP TEMPERATURE

Fig 3(b)

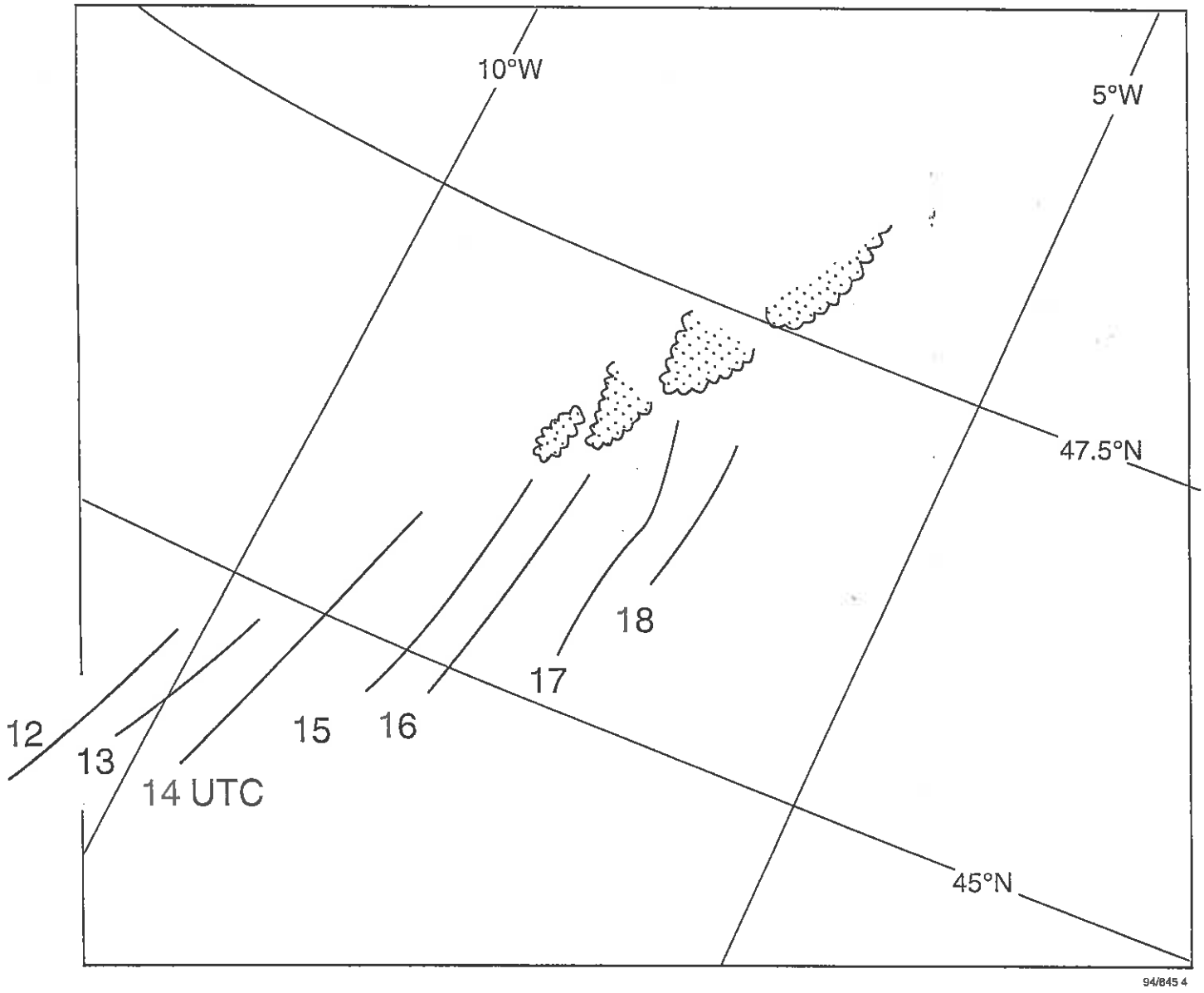

Fig 4

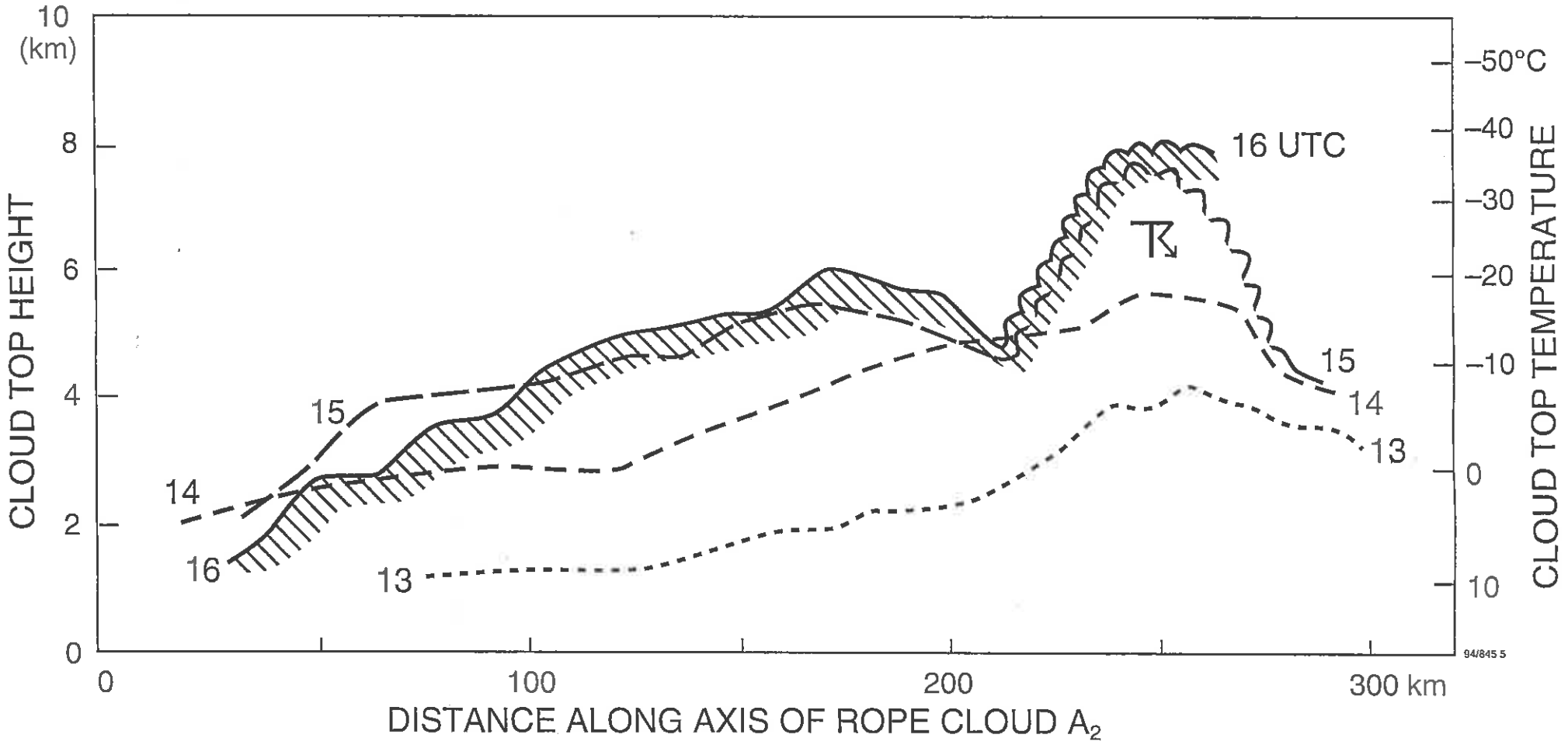
10
(km)
8
6
4
2
0
CLOUD TOP HEIGHT
–50°C
–40
–30
–20
–10
0
10
CLOUD TOP TEMPERATURE
16 UTC
15
14
13
15
14
16
13
94/845 5
0
100
200
300 km
DISTANCE ALONG AXIS OF ROPE CLOUD A2

Fig 5

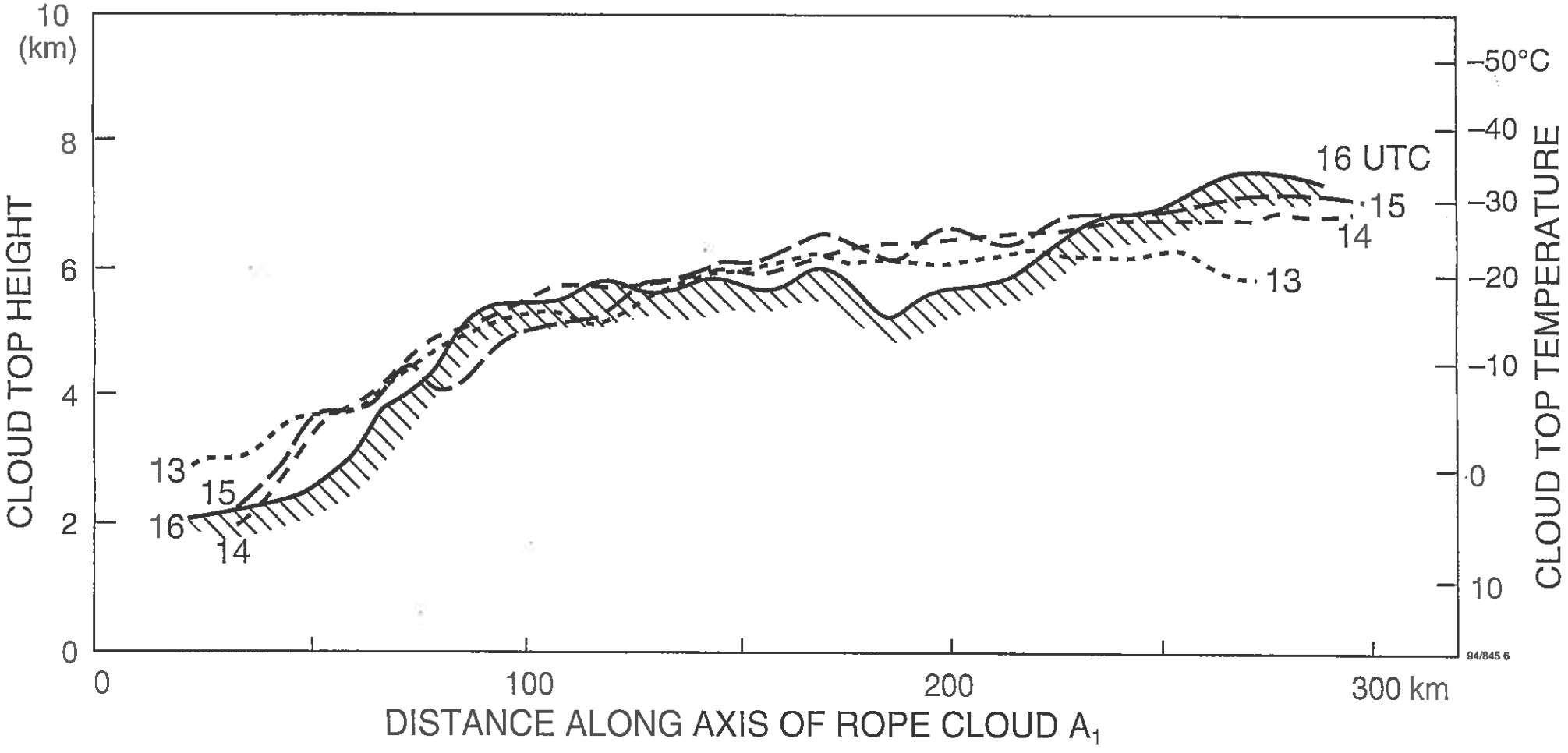
10
(km)
8
6
4
2
0
CLOUD TOP HEIGHT
−50°C
−40
−30
−20
−10
0
10
CLOUD TOP TEMPERATURE
16 UTC
15
14
13
13
15
16
14
94/845 6
0
100
200
300 km
DISTANCE ALONG AXIS OF ROPE CLOUD A1

Fig 6

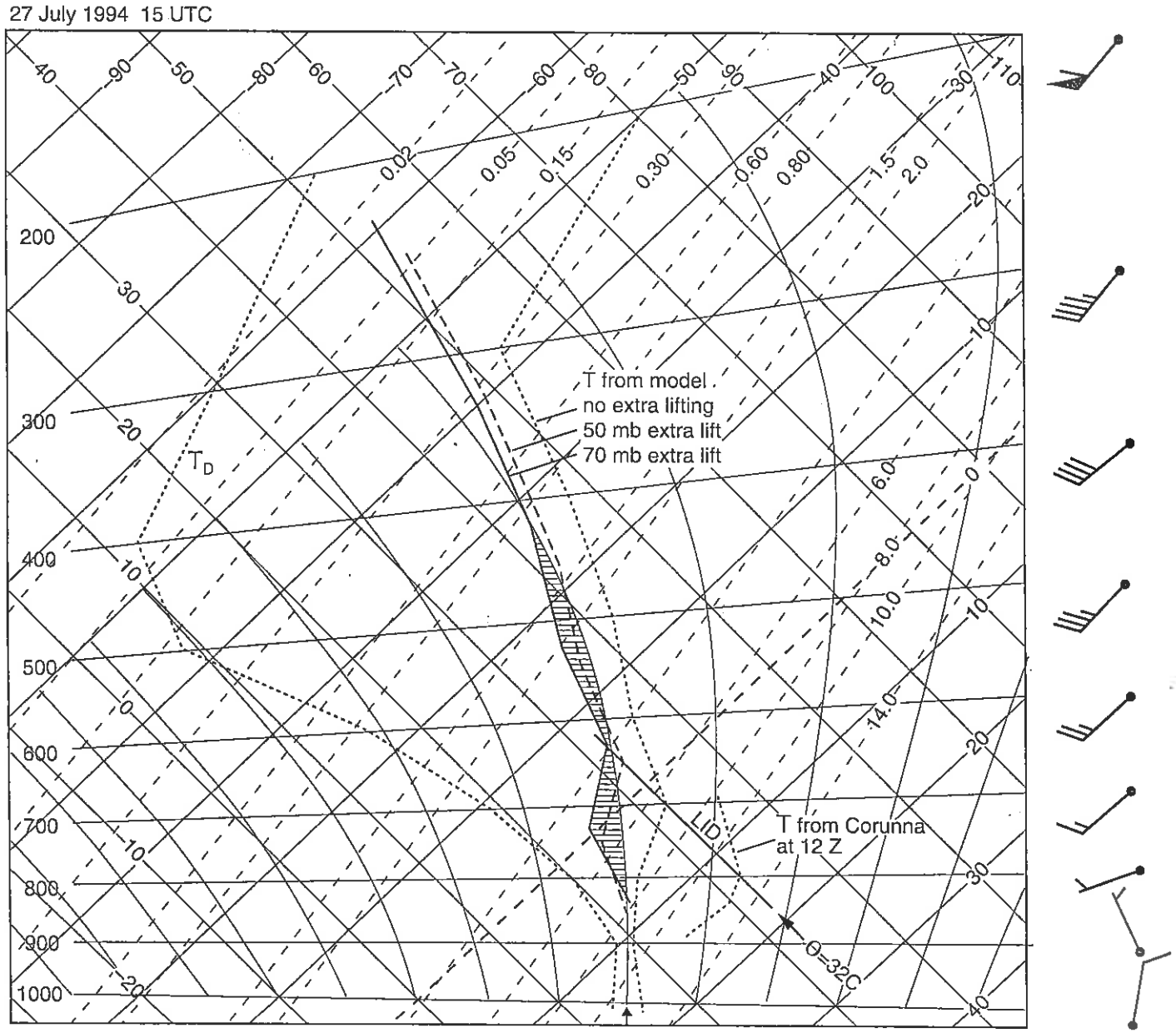
27 July 1994 15 UTC
T from model .
no extra lifting
50 mb extra lift
70 mb extra lift
T_D
LID
T from Corunna
at 12 Z
θ=32C
84/845 7

Fig 7

CURRENT JCMM INTERNAL REPORTS

This series of JCMM Internal Reports, initiated in 1993, contains unpublished reports and also versions of articles submitted for publication. The complete set of Internal Reports is available from the National Meteorology Library on loan, if required.

1. **Research Strategy and Programme.**
   K A Browning et al
   January 1993

2. **The GEWEX Cloud System Study (GCSS).**
   GEWEX Cloud System Science Team
   January 1993

3. **Evolution of a mesoscale upper tropospheric vorticity maximum and comma cloud from a cloud-free two-dimensional potential vorticity anomaly.**
   K A Browning
   January 1993

4. **The Global Energy and Water Cycle**
   K A Browning
   July 1993

5. **Structure of a midlatitude cyclone before occlusion.**
   K A Browning and N Roberts
   July 1993

6. **Developments in Systems and Tools for Weather Forecasting.**
   K A Browning and G Szejwach
   July 1993

7. **Diagnostic study of a narrow cold frontal rainband and severe winds associated with a stratospheric intrusion.**
   K A Browning and R Reynolds
   August 1993

8. **Survey of perceived priority issues in the parametrizations of cloud-related processes in GCMs.**
   K A Browning
   September 1993

9. **The Effect of Rain on Longwave Radiation.**
   I Dharssi
   September 1993

10. **Cloud Microphysical Processes - A Description of the Parametrization used in the Large Eddy Model.**
H Swann
July 1994

11. **An Appreciation of the Meteorological Research of Ernst Kleinschmidt.**
A J Thorpe
May 1992

12. **Potential Vorticity of Flow Along the Alps.**
A J Thorpe, H Volkert and Dietrich Heimann
August 1992

13. **The Representation of Fronts.**
A J Thorpe
January 1993

14. **A Parametrization Scheme for Symmetric Instability: Tests for an Idealised Flow.**
C S Chan and A J Thorpe
February 1993

15. **The Fronts 92 Experiment: a Quicklook Atlas.**
Edited by T D Hewson
November 1993

16. **Frontal wave stability during moist deformation frontogenesis. Part 1. Linear wave dynamics**
C H Bishop and A J Thorpe
May 1993

17. **Frontal wave stability during moist deformation frontogenesis. Part 2. The suppression of non-linear wave development.**
C H Bishop and A J Thorpe
May 1993

18. **Gravity waves in sheared ducts.**
S Monserrat and A J Thorpe
October 1993

19. **Potential Vorticity and the Electrostatics Analogy: Quasi-Geostrophic Theory.**
C Bishop and A J Thorpe
November 1993

20. **Recent Advances in the Measurement of Precipitation by Radar.**
A J Illingworth
April 1993

21. **Micro-Physique et Givrage. Cloud Microphysics and Aircraft Icing.**
A J Illingworth
May 1993

22. **Differential Phase Measurements of Precipitation.**
M Blackman and A J Illingworth
May 1993

23. **Estimation of Effective Radius of Cloud Particles from the Radar Reflectivity.**
N I Fox and A J Illingworth
May 1993

24. **A Simple Method of Dopplerising a Pulsed Magnetron Radar.**
L Hua, A J Illingworth and J Eastment
November 1993

25. **Radiation and Polar Lows.**
George C Craig
February 1994

26. **Collected preprints submitted to International Symposium on the Life Cycles of Extratropical Cyclones; Bergen, Norway, 27 June - 1 July 1994**
April 1994

27. **Convective Frontogenesis**
Douglas J Parker and Alan J Thorpe
April 1994

28. **Improved Measurement Of The Ice Water Content In Cirrus Using A Total Water Evaporator**
Philip R A Brown and Peter N Francis
April 1994

29. **Mesoscale Effects of a Dry Intrusion within a Vigorous Cyclone**
K A Browning and B W Golding
April 1994

30. **GEWEX Cloud System Study, Science Plan**
May 1994

31. **Parametrization of Momentum Transport by Convectively Generated Gravity Waves**
R Kershaw
May 1994

32. **Mesoscale Modelling Newsletter, No. 5**
May 1994

33. **Observations of the mesoscale sub-structure in the cold air of a developing frontal cyclone**
K A Browning, S A Clough, C S A Davitt, N M Roberts and T D Hewson
May 1994

34. **Longwave Radiative Forcing of a Simulated Tropical Squall Line**
Imtiaz Dharssi
July 1994

35. **On the nature of the convective circulations at a kata-cold front**
K A Browning
September 1994

36. **Collected preprints of papers submitted to the COST-75 International Seminar on Advanced Weather Radar Systems, Brussels, 20-23 September 1994**
November 1994

37. **Use of satellite imagery to diagnose events leading to frontal thunderstorms: Parts I and II of a case study**
K A Browning and N M Roberts
November 1994

Met Office Joint Centre for Mesoscale Meteorology Department of Meteorology
University of Reading PO Box 243 Reading RG6 6BB United Kingdom
Tel: +44 (0)118 931 8425 Fax: +44 (0)118 931 8791
www.metoffice.com